Slice Sampling with Multivariate Steps

by

Madeleine B. Thompson

A thesis submitted in conformity with the requirements
for the degree of Doctor of Philosophy
Graduate Department of Statistics
University of Toronto

Abstract

Slice Sampling with Multivariate Steps

Madeleine B. Thompson

Doctor of Philosophy

Graduate Department of Statistics

University of Toronto

2011

Markov chain Monte Carlo (MCMC) allows statisticians to sample from a wide variety of multidimensional probability distributions. Unfortunately, MCMC is often difficult to use when components of the target distribution are highly correlated or have disparate variances. This thesis presents three results that attempt to address this problem. First, it demonstrates a means for graphical comparison of MCMC methods, which allows researchers to compare the behavior of a variety of samplers on a variety of distributions. Second, it presents a collection of new slice-sampling MCMC methods. These methods either adapt globally or use the adaptive crumb framework for sampling with multivariate steps. They perform well with minimal tuning on distributions when popular methods do not. Methods in the first group learn an approximation to the covariance of the target distribution and use its eigendecomposition to take non-axis-aligned steps. Methods in the second group use the gradients at rejected proposed moves to approximate the local shape of the target distribution so that subsequent proposals move more efficiently through the state space. Finally, this thesis explores the scaling of slice sampling with multivariate steps with respect to dimension, resulting in a formula for optimally choosing scale tuning parameters. It shows that the scaling of untransformed methods can sometimes be improved by alternating steps from those methods with radial steps based on those of the polar slice sampler.

Acknowledgements

I would like to thank my advisor, Radford Neal, for his support with this thesis and the research leading up to it. Some material originally appeared in a technical report coauthored with him, "Covariance Adaptive Slice Sampling" (Thompson and Neal, 2010).

Contents

List of figures

Chapter 1

Introduction

1.1 Motivation

When researchers need to perform a statistical analysis, they usually reach for standard tools like t-tests, linear regression, and ANOVA. The results may not be easy to interpret correctly, but they are at least easy to generate. The methods have a gentle learning curve, allowing users with minimal sophistication to interpret the most straightforward aspects of their results. One can, for instance, make use of a regression line without understanding diagnostics like C_p (Mallows, 1973). As a user becomes more familiar with a method, they can draw richer conclusions and perform more subtle analyses. They do not need to understand the inner workings of the method the first time they use it. LOESS illustrates this phenomenon. While it has many free parameters, a LOESS fit can be computed entirely automatically. Users do not even know what they are estimating—they just ask their statistics software to fit a curve to their data.

It is my hope that this simplicity can be extended to a wider variety of models. Currently, balanced ANOVA is used more often than more general multilevel models of the sort described by Gelman et al. (2004, ch. 5) because the more general models must be specified in a language at least as complex as that of BUGS (Spiegelhalter et al.,

1995, §4). Users must learn to tune a Markov chain Monte Carlo (MCMC) sampler (Neal, 1993) and analyze the results for convergence. They must also learn how to display the simulation results in a way that can be understood. The MCMC sampler tuning step is the most difficult aspect of this procedure; each of the other steps must also be performed in ANOVA, which runs entirely automatically. The necessity of user involvement in fitting the model forces the user to manage the entire process themself. The hope that a wider variety of models could be fit with the ease of LOESS or ANOVA motivates the research described in this document.

In particular, this thesis focuses on the development of MCMC methods that are applicable to a wide variety of probability distributions without manual tuning. Most of those who use MCMC use some variation on Gibbs sampling (Neal, 1993, §4.1). Gibbs sampling is only possible when one knows the full conditional distributions of the components of the distribution, largely restricting its use to models with Gaussian, gamma, and binomial conditional distributions. Even on those models, it only performs well when those components are not highly correlated.

The class of models that can be modeled with Gibbs sampling can be expanded to allow for components with log-concave distributions of unknown form by applying adaptive rejection sampling (abbreviated ARS, Gilks and Wild, 1992). ARS requires users to specify an initial envelope for the conditional, though this can often be automatically determined. Further expansion to include those models with non-log-concave conditionals is possible with the use of adaptive rejection Metropolis sampling (abbreviated ARMS, Gilks et al., 1995). Like ARS, ARMS requires the user to specify an initial envelope, but with ARMS, a simulation could miss modes if the envelope is badly chosen. A proper envelope may depend on the values of the conditioning variables, so ARMS is also often difficult to properly configure. More commonly, users use random-walk Metropolis to update a single coordinate at a time, though it is often much less efficient than Gibbs sampling or ARMS and requires careful tuning.

An alternative to methods like ARMS and random-walk Metropolis, which require significant tuning, is methods like adaptive Metropolis (Haario et al., 2001), which attempt to learn a suitable proposal distribution from previous states instead of requiring the user to specify one a priori. Adaptive Metropolis can update multiple components of the state space simultaneously, and by learning the covariance matrix of the target distribution, it can perform well even when the components are highly correlated. However, it is not acceptable to indiscriminately adapt a proposal distribution. Even if each individual step holds the target distribution invariant, the resulting sequence of states may not converge to the intended distribution once adaptation is taken into account. Roberts and Rosenthal (2007) discuss this issue in greater depth. A second concern with adaptive methods is that they may be difficult to embed in a larger scheme. For example, if one knows the full conditional for some subset of the components and wishes to update the remaining ones with adaptive Metropolis, the adaptive state may be inappropriate because the target distribution, as seen by adaptive Metropolis, may change shape when the conditioning variables change.

One promising approach to MCMC sampling when Gibbs sampling is not feasible is slice sampling, which is more robust to peculiarities of target distributions than most MCMC samplers (Roberts and Rosenthal, 1999). Slice sampling with univariate updates (Neal, 2003, §4) is used as an alternative to ARMS and random-walk Metropolis to update individual components of a simulation in turn. Like these two methods, it only uses the log density of the target distribution, so it is not limited to distributions that factor into conditional distributions of known, simple forms like Gibbs sampling is. And, it is robust to poorly chosen tuning parameters.

However, like any method that only updates one component at a time, slice sampling with univariate updates will not be efficient when the components of the target distribution are highly correlated. Neal (2003, §5) also proposes several variations of slice sampling with multivariate steps, but they largely share this weakness. This thesis

extends his work on multivariate steps and proposes several slice sampling methods that take multivariate steps that respect the local shape of the target distribution. Using either previously visited states or the gradient of the log density at rejected moves, these slice samplers can be efficient even when the distribution is badly scaled and the parameters are highly correlated, which is often the case with the multivariate models I hope to make more broadly accessible.

In high-dimensional spaces, some methods that update multiple components at once can move efficiently along the contours of a target distribution but not between them. Roberts and Rosenthal (2002) propose the "polar slice sampler," a variation of slice sampling that operates in polar coordinates relative to a single, known mode. In this coordinate system, the sampler mixes efficiently with respect to the log density. However, the polar slice sampler uses non-adaptive rejection sampling to draw proposed moves, which is often prohibitively inefficient, so it has not been used much. This thesis extends the work of Roberts and Rosenthal, developing a practical means to modify an MCMC method so that it can move efficiently between contours of a target distribution. The proposed methods take radial steps similar to those of the polar slice sampler, but use a secondary MCMC method to move in the angular coordinates so that rejection sampling is not needed.

Development of new MCMC methods motivated another question: how can we identify the circumstances under which one MCMC method is superior to other methods? To address this, I propose several figures of merit for MCMC samplers and develop schemes for presenting the merits of a range of samplers and test distributions so that I and other researchers can place newly developed methods in a broader context.

1.2 Outline

Chapter 2 compares figures of merit for MCMC samplers and the means to present them. First, I discuss how the mixing efficiency of a Markov chain can be described by its autocorrelation time and describe several methods for estimating this. I describe a test set developed for these methods, which I use to justify a preference for a method that models a Markov chain as an autoregressive process. Autocorrelation time only considers the state sequence of a Markov chain, not the resources used to compute it, so it is not an acceptable figure of merit on its own. I describe how one can build on autocorrelation time to compute a more appropriate figure of merit, log density function evaluations per uncorrelated observation. Then, I demonstrate how this measure can be used to make graphical comparisons of collections of MCMC methods with a range of tuning parameters on several distributions simultaneously. These comparisons allow researchers to see how particular MCMC methods fit into a broader context.

Chapter 3 contains the principal results of this research, several variations on slice sampling that take multivariate steps. The first two methods are inspired by adaptive Metropolis. They adaptively choose slice approximations using the eigendecomposition of the sample covariance matrix of the target distribution. These methods often work well, but have limitations that come from retaining state from iteration to iteration. To address these, I first describe a simple but unworkable method that uses gradients at rejected points to create a temporary polyhedral approximation to the slice. It is computationally infeasible, but motivates the use of the crumb framework, which allows for methods with more computationally tractable proposal distributions. I then describe one such method in the crumb framework, covariance matching. Using log density gradients at rejected proposals, covariance matching chooses crumb distributions so that the covariances of the proposal distributions approximate the covariance of uniform sampling over the slice. This is followed by a description of a second method in the crumb framework, shrinking rank, which also uses gradients to adapt to local structure of the target distribution. It

is more computationally efficient and simpler than covariance matching, and retains its most desirable properties. The chapter closes with a comparison of the proposed MCMC methods using the evaluation methods of chapter 2.

While chapter 3 focuses on efficient sampling with respect to linear functions of the components of the state space of the target distribution, chapter 4 focuses on efficient sampling with respect to the log density of the target distribution and addresses the closely related topic of scaling with increasing dimension. It describes experiments that explore the scaling behavior and proper tuning of samplers in the crumb framework. It shows that samplers in the crumb framework commonly have linear scaling with respect to the dimension of the target distribution and that this can be improved under some circumstances. It extends these results to more practical samplers, showing how combining univariate radial steps with a method like covariance matching can result in improved scaling with respect to log density.

Finally, chapter 5 describes the circumstances under which both the MCMC methods and the techniques used to analyze them may be more broadly applied. It also provides references to software that implements the methods described in this document.

Chapter 2

Measuring sampler efficiency

To compare the performance of MCMC methods using a collection of simulations, we must be able to quantify the efficiency of a single simulation, and we must have a means to display a collection of these measurements. In this chapter, I break down the efficiency of a simulation into measurements of the correlation between observations and the cost of obtaining an observation. Then, I demonstrate several types of plots for comparing the efficiency of collections of simulations representing different samplers, distributions, and tuning parameters.

2.1 Autocorrelation time

Autocorrelation time measures the convergence rate of the sample mean of a function of a stationary, geometrically ergodic Markov chain with finite variance. Let $\{X_i\}_{i=1}^n$ be n values of a scalar function of the states of such a Markov chain, where $EX_i = \mu$ and $\operatorname{var} X_i = \sigma^2$. Let $\bar{X}_n$ be the sample mean of $(X_1, \ldots, X_n)$. Then, the autocorrelation time is the value of τ such that:

$$\sqrt{\frac{n}{\tau}} \cdot \frac{\bar{X}_n - \mu}{\sigma} \Longrightarrow N(0,1) \tag{2.1}$$

Conceptually, the autocorrelation time is the number of Markov chain transitions equivalent to a single uncorrelated draw from the distribution of $\{X_i\}$. It can be a useful summary of the efficiency of an MCMC sampler. However, one must be cautious when using it with adaptive methods such as those discussed in section 3.2 because they do not have stationary distributions, and equation 2.1 does not strictly apply.

Since there is rarely a closed-form expression for the autocorrelation time, many methods for estimating it from sampled data have been developed. The following sections describe four such methods in wide use: computing batch means, fitting a linear regression to the log spectrum, summing an initial sequence of the sample autocorrelation function, and modeling as an autoregressive process. Then, these methods are compared on a test set of seven series. For a broader context, two classic overviews of uncertainty in MCMC estimation are Geyer (1992) and Neal (1993, §6.3). An alternative to autocorrelation time, potential scale reduction, is discussed by Gelman and Rubin (1992).

2.1.1 Batch mean estimator

Equation 2.1 is approximately true for a finite sequence, so one can obtain multiple estimates of the mean by dividing the $\{X_i\}$ into non-overlapping batches of size m and computing the sample mean of each batch. The asymptotic variance of each batch mean as m goes to infinity is $\sigma^2/(m/\tau)$. So, if s^2 is the sample variance of $\{X_i\}$ and s_m^2 is the sample variance of the batch means, one can estimate the autocorrelation time with:

$$\hat{\tau}_{n,m} = m\frac{s_m^2}{s^2} \tag{2.2}$$

For this to be a consistent estimator of τ, the batch size and the number of batches must go to infinity. To ensure this, I use $n^{1/3}$ batches of size $n^{2/3}$. Fishman (1978, §5.9) discusses batch means in great detail; Neal (1993, p. 104) and Geyer (1992, §3.2) discuss batch means in the context of MCMC.

2.1.2 Least squares fit to the log spectrum

In the spectrum fit method (Heidelberger and Welch, 1981, §2.4), a linear regression is fit to the lower frequencies of the log-spectrum of the chain and used to compute an estimate of the spectrum at frequency zero, denoted by $\hat{I}_0$. Let s^2 be the sample variance of the $\{X_i\}$. The autocorrelation time can be estimated as:

$$\hat{\tau} = \frac{\hat{I}_0}{s^2} \tag{2.3}$$

This is implemented by the `spectrum0` function in R's CODA package (Plummer et al., 2006). First and second order polynomial fits are practically indistinguishable on the test series described in section 2.1.5, so I only include the results for a first order fit.

2.1.3 Initial sequence estimators

One formula for the autocorrelation time is (Straatsma et al., 1986, p. 91):

$$\tau = 1 + 2\sum_{k=1}^{\infty} \rho_k \tag{2.4}$$

where ρ_k is the autocorrelation function (ACF) of the series at lag k. For small lags, ρ_k can be estimated with:

$$\hat{\rho}_k = \frac{1}{ns^2}\sum_{i=1}^{n-k}(X_i - \bar{X}_n)(X_{i+k} - \bar{X}_n) \tag{2.5}$$

But, $\hat{\rho}_k$ is not defined when k is greater than $n-1$, and the partial sum $\hat{\rho}_1 + \cdots + \hat{\rho}_{n-1}$ does not have a variance that goes to zero as n goes to infinity, so substituting all values from equation 2.5 into equation 2.4 is not an acceptable way to estimate τ.

One approach to this problem, initial sequence estimators, was created by Geyer (1992). He shows that, for reversible Markov chains, sums of pairs of consecutive ACF values, $\rho_i + \rho_{i+1}$, are always positive. He obtains a consistent estimator, the initial positive sequence (IPS) estimator, by truncating the sum when the sum of adjacent sample ACF values is negative, indicating that at that point ACF estimates are dominated by noise.

Further, the sequence of sums of pairs is always decreasing, so one can smooth the initial positive sequence when a sum of two adjacent sample ACF values is larger than the sum of the previous pair; the resulting estimator is the initial monotone sequence (IMS) estimator. Finally, the sequence of sums of pairs is also convex. Smoothing the sum to account for this results in the initial convex sequence (ICS) estimator. For more details, see Geyer (1992, §3.3). I was unable to distinguish the behavior of the IPS, IMS, and ICS estimators on the series of section 2.1.5, so the comparisons of section 2.1.6 only include the ICS estimator.

2.1.4 AR process estimator

Another way to estimate the autocorrelation time, based on CODA's `spectrum0.ar` (Plummer et al., 2006), is to model the series as an autoregressive (AR) process of order p, with p chosen by AIC. Consider a model of the form:

$$X_t = \mu + \pi_1 X_{t-1} + \cdots + \pi_p X_{t-p} + a_t, \qquad a_t \sim N(0, \sigma_a^2) \tag{2.6}$$

Let $\hat{\rho}_{1:p}$ be the vector $(\hat{\rho}_1, \ldots, \hat{\rho}_p)$. The Yule–Walker method (Wei, 2006, pp. 136–138) can be used to obtain an estimate of the AR coefficients, $\hat{\pi}_{1:p}$, using $\hat{\rho}_{1:p}$. Combining equations 7.1.5 and 12.2.8b of Wei (2006, pp. 137, 274–275), the autocorrelation time can be estimated with:

$$\hat{\tau} = \frac{1 - \hat{\rho}_{1:p}^T \hat{\pi}_{1:p}}{\left(1 - 1_p^T \hat{\pi}_{1:p}\right)^2} \tag{2.7}$$

This is a consistent estimator for τ as n goes to infinity if AIC increases p along with n, with p increasing more slowly than n so that errors in the coefficient estimates do not dominate the estimate of $\hat{\tau}$. (This does not include the case where an AR(p) model with finite p generated the data, but that case is not important.) For more information on the AR process method, see Fishman (1978, §5.10).

Because the Yule–Walker method also estimates the asymptotic variance of $\hat{\pi}_{1:p}$, denoted by V_π, Monte Carlo simulation can be used to generate a confidence interval for

the autocorrelation time. Draw $(\pi^{(1)}, \pi^{(2)}, \ldots)$ from the distribution:

$$\pi^{(i)} \sim N(\hat{\pi}_{1:p}, V_\pi) \tag{2.8}$$

When the roots of $1 = \pi_1^{(i)} z + \cdots + \pi_p^{(i)} z^p$ all lie outside the unit circle, $\pi^{(i)}$ produces a stationary time series (Wei, 2006, p. 47, equation 3.1.28). The corresponding autocorrelation function, $\rho^{(i)}$, can be computed with the R function `ARMAacf`. Substituting $\pi^{(i)}$ and $\rho^{(i)}$ into equation 2.7 gives a simulated draw from the distribution of $\hat{\tau}$. When at least one root lies inside or on the unit circle, $\pi^{(i)}$ produces a nonstationary process (Wei, 2006, p. 26), and τ is not defined; an estimate of infinity is used in this case. After simulating a sample of a reasonable size, the quantiles of the sample can be used as a confidence interval for τ. If more than 2.5% of the simulated $\pi^{(i)}$ define nonstationary processes, the resulting 95% confidence interval is unbounded.

2.1.5 Seven test series

I evaluate the methods described in sections 2.1.1, 2.1.2, 2.1.3, and 2.1.4 with seven series. The first 10,000 elements of each are plotted in figure 2.1.

- **AR(1)** is an AR(1) process with an autocorrelation of 0.98 and uncorrelated standard Gaussian errors. From equation 2.7, its autocorrelation time is 99. It is, in one sense, the simplest possible series with an autocorrelation time other than one.

- **AR(2)** is an AR(2) process with poles at $-1 + 0.1i$ and $-1 - 0.1i$:

$$Z_t = 1.98\, Z_{t-1} - 0.99\, Z_{t-2} + a_t, \quad a_t \sim N(0, 1) \tag{2.9}$$

  Despite oscillating with a period of about 60, the terms in its autocorrelation function nearly cancel each other out, so its autocorrelation time is approximately two. This series is included to identify methods that cannot identify cancellation in long-range dependence.

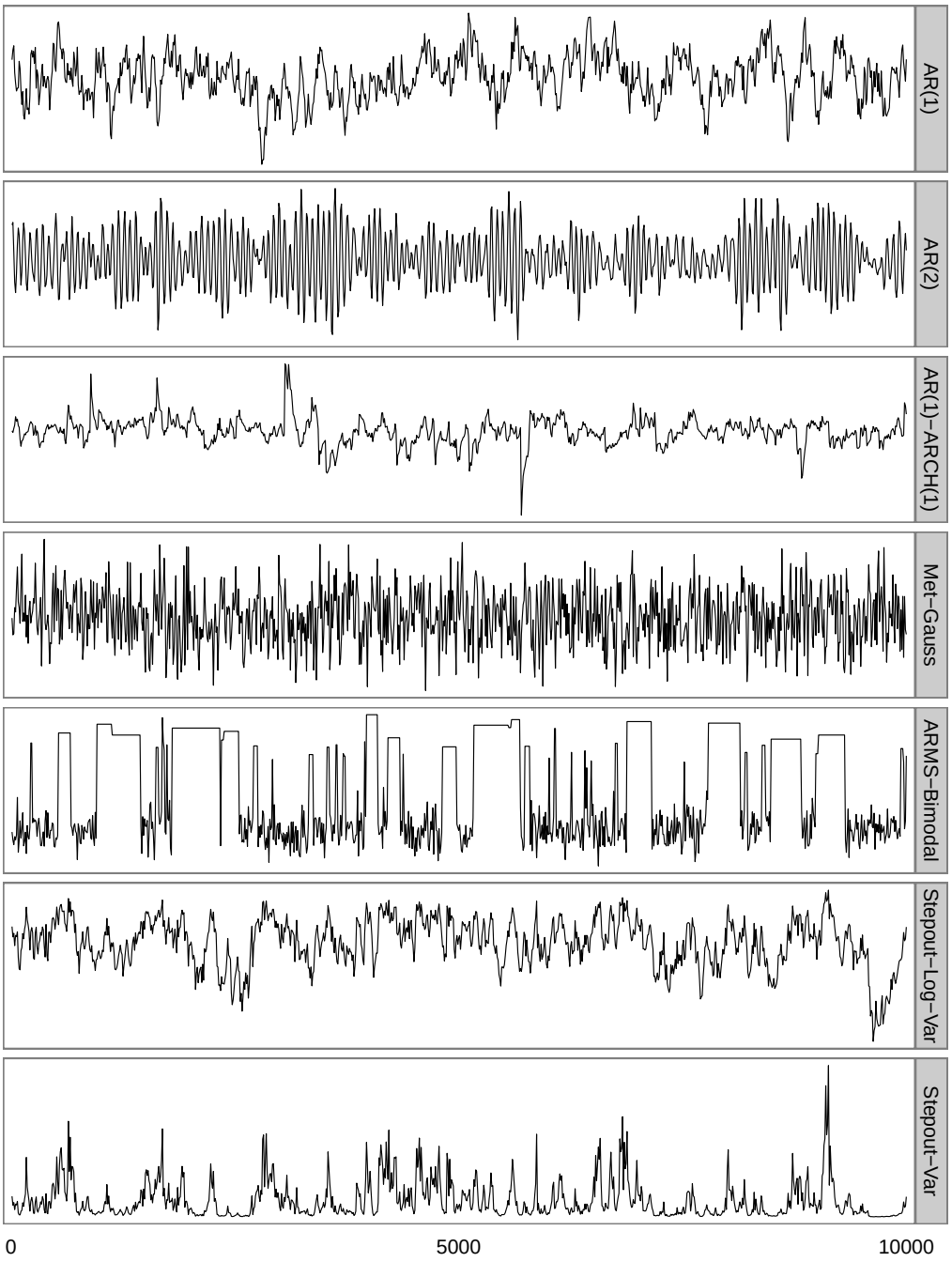

Figure 2.1: The first 10,000 elements of seven series used as a test set. See section 2.1.5 for discussion.

- **AR(1)-ARCH(1)** is an AR(1) process with autocorrelation of 0.98 and autocorrelated errors:

$$Z_t = 0.98\, Z_{t-1} + a_t, \quad a_t \sim N\left(0, 0.01 + 0.99\, a_{t-1}^2\right) \tag{2.10}$$

  Its autocorrelation time is also 99. This series could confound methods that assume constant step variance.

- **Met-Gauss** is a sequence of states generated by a Metropolis sampler with standard Gaussian proposals sampling from a standard Gaussian target distribution. It has a proposal acceptance rate of 0.7 and an autocorrelation time of eight. It is a simple example of a state sequence from an MCMC sampler.

- **ARMS-Bimodal** is also a sequence of states from an MCMC simulation, ARMS (Gilks et al., 1995) applied to a mixture of two Gaussians. The sampler is badly tuned, so it rarely accepts a proposal when near the upper mode. It has an autocorrelation time of approximately 200.

- **Stepout-Log-Var** is a third MCMC sequence, the log-variance parameter of slice sampling with stepping out (Neal, 2003, §4) sampling from a ten-parameter multilevel model (Gelman et al., 2004, pp. 138–145). Its autocorrelation time is approximately 200.

- **Stepout-Var** was generated by exponentiating the states of Stepout-Log-Var. Because its sample mean is dominated by large observations, its autocorrelation time, approximately 100, is different than that of Stepout-Log-Var. Like ARMS-Bimodal and Stepout-Log-Var, it is a challenging, real-world example of a sequence whose autocorrelation time might be unknown.

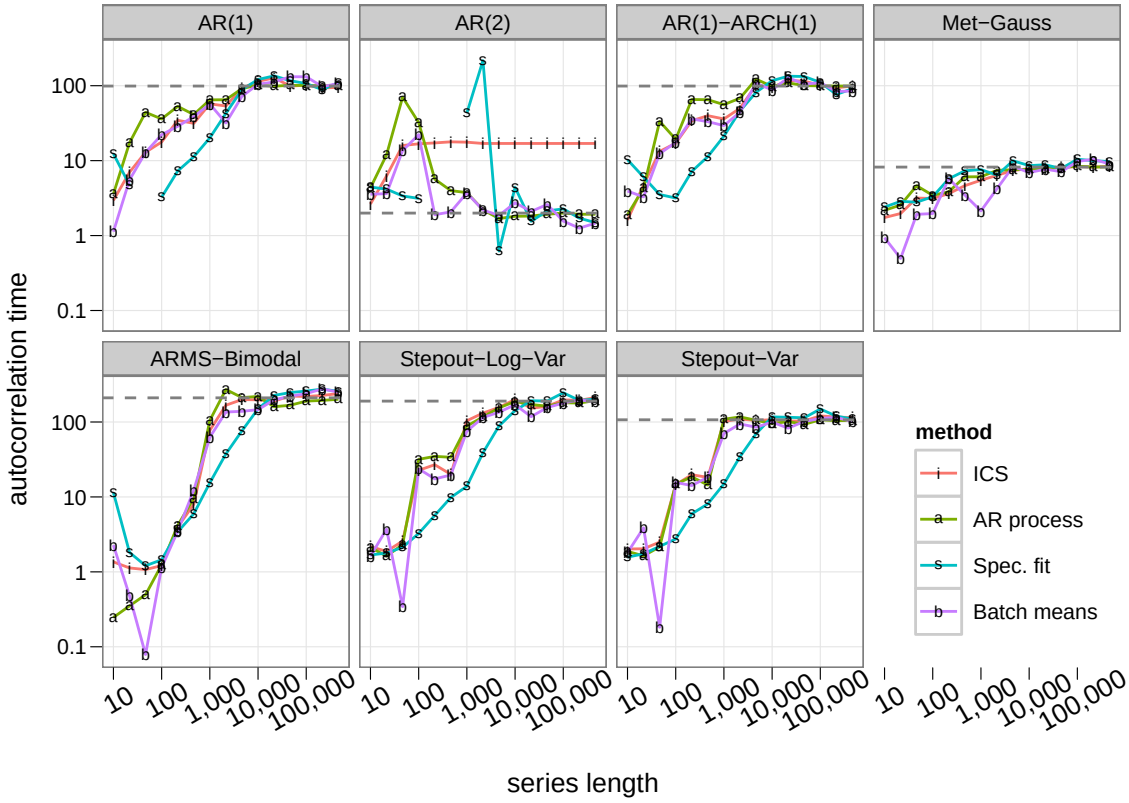

Figure 2.2: Autocorrelation times computed by four methods on seven series for a range of subsequence lengths. Each plot symbol represents a single estimate. The dashed line indicates the true autocorrelation time. Breaks in the lines for spectrum fit indicate instances where the method failed to produce an estimate. See section 2.1.6 for discussion.

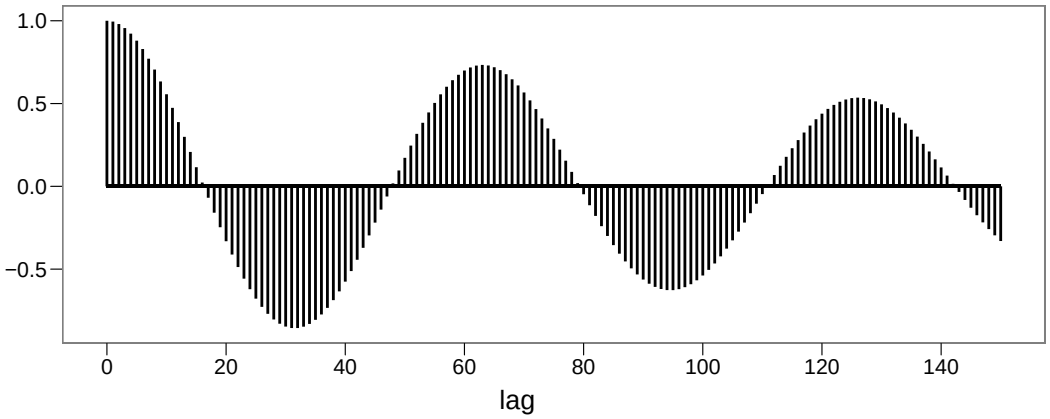

Figure 2.3: The autocorrelation function of the AR(2) series. See section 2.1.6 for discussion.

2.1.6 Comparison of autocorrelation time estimators

This section compares the true autocorrelation time of each series to the autocorrelation time estimated by each method for subsequences ranging in length from 10 to 500,000. The results are plotted in figure 2.2. All four methods converge to the true value on all seven chains, with the exception of ICS on the AR(2) process. In general, the AR process method converges to the true autocorrelation time fastest, followed by ICS, batch means, and finally spectrum fit, which does not even produce an estimate in all cases. All four methods tend to underestimate autocorrelation times for all short sequences except those from the AR(2) process, which appears in small samples to have a longer autocorrelation time than it actually does.

ICS is inconsistent on the AR(2) process because the autocorrelation function of the AR(2) process is significant at lags larger than its first zero-crossing (see figure 2.3). ICS and the other initial sequence estimators are not necessarily consistent when the underlying chain is not reversible; the AR(2) process is not, when considered as a two state system with the Markov property. These estimators stop summing the sample

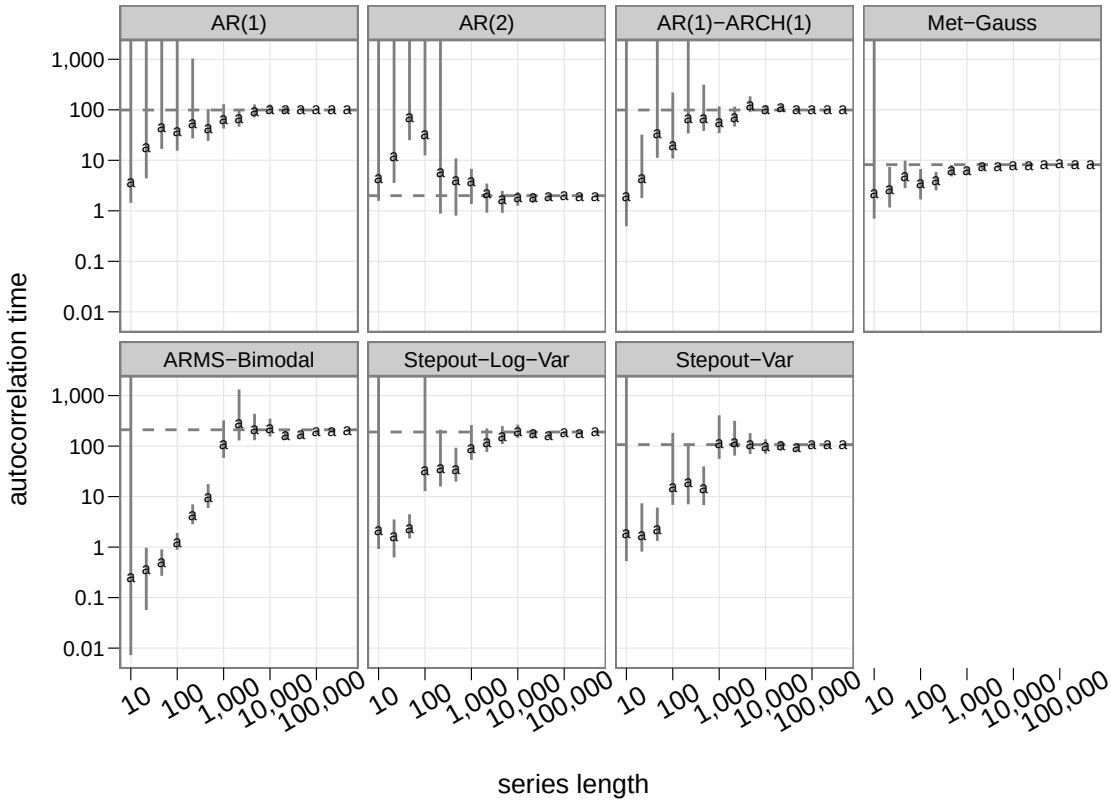

Figure 2.4: AR process-generated point estimates and 95% confidence intervals for the autocorrelation times of seven series for a range of subsequence lengths. The dashed line indicates the true autocorrelation time. The confidence intervals are somewhat reasonable. See section 2.1.6 for discussion.

autocorrelation function the first time its values fall below zero, so these estimators never see that negative values at large lags cancel positive values at small lags.

The AR process method can also generate approximate confidence intervals for the autocorrelation time. 95% confidence intervals generated by the AR process method are shown in figure 2.4. The intervals are somewhat reasonable for subsequences longer than the true autocorrelation time for series other than AR(2), where the first few hundred elements do not represent the entire series but appear as though they might. Even on the others, they are only accurate enough to be used as a rough diagnostic.

The AR process method is marginally more accurate than the three other methods and is the only method that, as implemented, generates confidence intervals, so I usually prefer it to the other three. The batch mean estimate is faster to compute and almost as accurate, so it is useful when speed is important and confidence intervals are not necessary.

2.1.7 Multivariate distributions

So far, I have considered the estimation of autocorrelation time for a scalar function of the state of a Markov chain. Often, however, users are interested in how fast the Markov chain as a whole mixes. Let Y be a linear combination of two scalar functions of state, $X^{(1)}$ and $X^{(2)}$:

$$Y = aX^{(1)} + bX^{(2)} \tag{2.11}$$

If the two functions have autocorrelation times $\tau^{(1)}$ and $\tau^{(2)}$, the variance of the sample mean of Y will be:

$$\begin{aligned}
\operatorname{var}(\bar{Y}_n) &= a^2 \operatorname{var}(\bar{X}_n^{(1)}) + 2ab \operatorname{cov}(\bar{X}_n^{(1)}, \bar{X}_n^{(2)}) + b^2 \operatorname{var}(\bar{X}_n^{(2)}) && (2.12)\\
&= a^2 \operatorname{var}(\bar{X}^{(1)}) + 2ab\sqrt{\operatorname{var}(\bar{X}^{(1)}) \operatorname{var}(\bar{X}^{(2)})} \operatorname{corr}(\bar{X}_n^{(1)}, \bar{X}_n^{(2)}) + b^2 \operatorname{var}(\bar{X}^{(2)}) \\
&\approx a^2 \frac{\tau^{(1)}}{n} \operatorname{var}(X^{(1)}) + 2ab \frac{\sqrt{\tau^{(1)}\tau^{(2)}}}{n} \sqrt{\operatorname{var}(X^{(1)}) \operatorname{var}(X^{(2)})} \operatorname{corr}(\bar{X}_n^{(1)}, \bar{X}_n^{(2)}) && (2.13)\\
&\quad + b^2 \frac{\tau^{(2)}}{n} \operatorname{var}(X^{(2)}) \\
&= \frac{1}{n} \left(\tau^{(1)} A + 2\sqrt{\tau^{(1)} A}\sqrt{\tau^{(2)} B} \operatorname{corr}(\bar{X}_n^{(1)}, \bar{X}_n^{(2)}) + \tau^{(2)} B \right) && (2.14)\\
&\leq \frac{4}{n} \max\left(\tau^{(1)} A, \tau^{(2)} B \right) && (2.15)
\end{aligned}$$

where $A = a^2 \operatorname{var} X^{(1)}$ and $B = b^2 \operatorname{var} X^{(2)}$. If the terms of the combination are not anti-correlated (so that there is no possibility the sample means cancel each other out) and the sample means come from independent observations, the variance of the sample mean of Y is asymptotically bounded below by $\frac{1}{n}(A + B)$. The bound of equation 2.15 is at most a factor of $4 \cdot \max(\tau^{(1)}, \tau^{(2)})$ larger, so unless the terms of the combination are

constructed to cancel each other out, the autocorrelation time of a linear combination of scalar functions of state is itself bounded by four times the autocorrelation time of the slowest mixing term.

More generally, unless the terms are constructed to cancel each other out, the autocorrelation time of an arbitrary linear combination of k components of the state of a Markov chain is, to a factor of $2k$, bounded above by the autocorrelation time of the slowest-mixing component of the state. So, it is usually appropriate to estimate autocorrelation times for each component of state and to describe the chain as a whole by the largest of these estimates. This document will take that approach.

Nonlinear functions of multiple components—or even a single component—may have substantially different autocorrelation times than those of any linear combination of components. The mixing rates of all possible functions of state cannot be summarized in a single number; additional information about which functions are relevant is necessary. One particular nonlinear function that may be of interest is the log density; its autocorrelation time is discussed in chapter 4.

2.2 Framework for comparing methods

2.2.1 MCMC methods for comparison

To demonstrate comparison of MCMC methods, I use the following four samplers, each of which has a single tuning parameter:

- **Step-out Slice** is slice sampling with stepping out, updating each coordinate sequentially, as described by Neal (2003, §4). The tuning parameter is w, the initial estimate of slice size.

- **Adaptive Metropolis** is described by Roberts and Rosenthal (2009, §2) and is based on an algorithm of Haario et al. (2001). The tuning parameter is the a scaling

factor for the standard deviation of the non-adaptive component of the proposal distribution, which they fix at 0.1 in their equation 2.1. This version of Metropolis uses multivariate Gaussian proposals with a covariance matrix determined by previous states. Unlike the version of Roberts and Rosenthal, this implementation stops adapting after a burn-in period. As in Roberts and Rosenthal, the probability of non-adaptive steps, β, is fixed at 0.05 unless otherwise specified.

- **Univariate Metropolis** is Metropolis with transitions that update each coordinate sequentially. The proposals are Gaussians centered at the current state with standard deviation equal to the tuning parameter.

- **Nonadaptive Crumb** is slice sampling with Gaussian crumbs (Neal, 2003, §5.2), a variant of slice sampling that takes multivariate steps and is the basis for the samplers described in sections 3.4 and 3.5. The tuning parameter is the standard deviation of the first crumb. Section 4.1 discusses its tuning in detail; here, θ is fixed at 0.95.

2.2.2 Distributions for comparison

These samplers are compared on the four distributions:

- **GP (unlogged)** is the posterior distribution of a Bayesian one-dimensional Gaussian process model with three parameters: two variance components and a correlation decay rate. The covariance between observations at x_i and x_j is:

$$\sigma_{ij} = \sigma_n^2 1_{i=j} + \sigma_f^2 \exp\left\{-\frac{(x_i - x_j)^2}{\rho}\right\} \tag{2.16}$$

  Observations at 30 random values on $[0, 1]$ are drawn with $(\sigma_n^2, \sigma_f^2, \rho) = (0.01, 1, 0.1)$; the distribution is the posterior for these three parameters given the observations and lognormal priors on each parameter. The contours of the distribution of the parameters are not axis-aligned. The distribution is right skewed in all parameters.

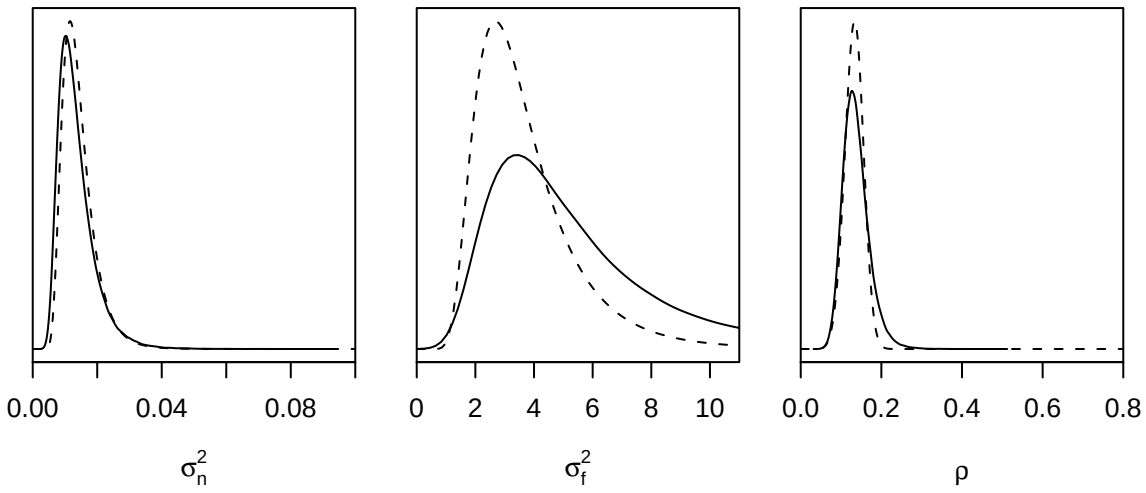

Figure 2.5: The marginal distributions (solid) and conditional distributions at the marginal mean (dashed) of the GP (unlogged) distribution. See section 2.2.2 for discussion.

The posterior marginal and conditional distributions of the three components are plotted in figure 2.5.

- $\boldsymbol{N_4(\rho = 0.999)}$ is a four dimensional Gaussian centered at $(1, 2, 3, 4)$ with covariance matrix:

$$\Sigma = \begin{bmatrix} 1 & 0.999 & 0.999 & 0.999 \\ 0.999 & 1 & 0.999 & 0.999 \\ 0.999 & 0.999 & 1 & 0.999 \\ 0.999 & 0.999 & 0.999 & 1 \end{bmatrix} \tag{2.17}$$

  Σ has a condition number of 2870.

- **Eight Schools** is a multilevel model in ten dimensions, consisting of eight group means and hyperparameters for their mean and log-variance (Gelman et al., 2004, pp. 138–145). Its covariance is well-conditioned.

- **German Credit** (Girolami and Calderhead, 2011, p. 15) is a Bayesian logistic regression with twenty-five parameters. Its data matrix is not standardized.

2.2.3 Processor time and log density evaluations

Before comparing performance of methods on a distribution, we must choose a measure of cost. Here, the methods of section 2.2.1 and distributions of section 2.2.2 are used to justify the choice of log-density evaluations per MCMC iteration multiplied by autocorrelation time.

If a user's goal is to estimate a parameter to a specific accuracy, they would want to choose an MCMC method that minimizes processor time per iteration multiplied by autocorrelation time. However, processor time measurements made on a researcher's machine depend on idiosyncratic factors such as the type of machine the researcher is using, other simultaneous tasks running on the machine, etc. Even identically configured simulations may generate different results.

An alternative to measuring processor usage is counting log-density function evaluations. Initialized with the same random seed, an MCMC simulation would evaluate this function the same number of times on machines of different speeds, on the same machine with different concurrent processes, and often even when implemented in different programming languages. However, this measure does not capture the overhead of the MCMC method, nor does it capture different ways a distribution can be represented to the method. For example, some methods require gradients to be computed, increasing the processor time per evaluation; some methods, such as Gibbs sampling, do not compute log densities at all.

To see the comparability of these two measures, at least on the distributions and methods described in sections 2.2.1 and 2.2.2, see figure 2.6, which plots the ratio of processor usage to log-density function evaluations for those samplers and distributions and for a range of tuning parameters. The ratios are normalized to the median processor time for a function evaluation over the simulations of that distribution. If processor usage and log density evaluations were perfectly comparable, every plotted point would lie on the dashed horizontal line indicating a ratio of one. For the simulations in figure 2.6, the

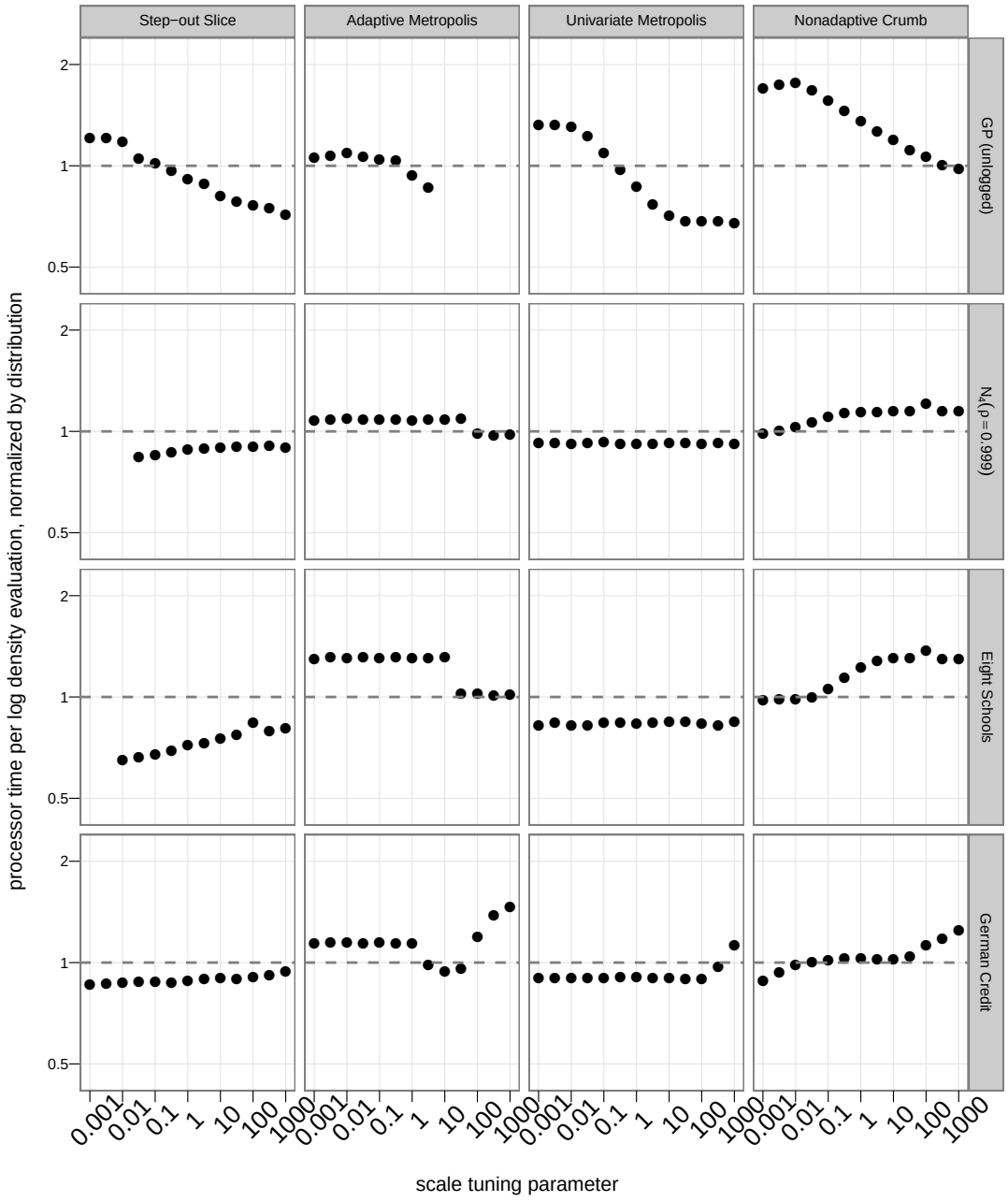

Figure 2.6: The ratio of processor usage to log density evaluations, normalized by distribution. One can see that this ratio does not depend much on method choice or tuning parameter; see section 2.2.3 for discussion. Each simulation is of length 250,000. The gaps in some of the plots correspond to incomplete simulations.

measures are at most a small multiple off from each other. Even though the overhead of Adaptive Metropolis, which is implemented in R and performs expensive matrix manipulations, is much larger than that of Nonadaptive Crumb, which is implemented in C and does not perform any expensive computations, the log density evaluations dominate the cost. Because no significant differences in ratios are observed, I am inclined to believe that comparing processor usage and comparing log density evaluations will yield similar conclusions regarding the merits of various MCMC methods.

2.3 Graphical comparison of methods

The cost measure described in section 2.2.3, evaluations per uncorrelated observation, provides a way of quantifying the performance of the MCMC methods described in section 2.2.1 on the distributions described in section 2.2.2. I simulated each of these distributions with each sampler for nine values of the sampler's tuning parameter in the range 0.001 to 1000. Each chain had a length of 250,000. Treating the first half of each chain as a burn-in period, I computed the autocorrelation time of each simulation using the AR process method of section 2.1.4 and multiplied it by the average number of log density evaluations the simulation needed per iteration to generate an estimate of the number of log density evaluations per uncorrelated observation. Smaller values indicate better performance. In this section and subsequent ones, I use the true mean instead of the sample mean when estimating autocorrelation times to reduce the chance that an erroneously low autocorrelation time will be estimated if a chain appears to have converged but has not.

In figure 2.7, I compare the evaluations per uncorrelated observation by plotting them as dots, with 95% simulation-based confidence intervals, against the tuning parameter for each combination of distribution and method. Question marks indicate simulations with too few unique states to identify an AR model. This occurs when Adaptive Metropolis

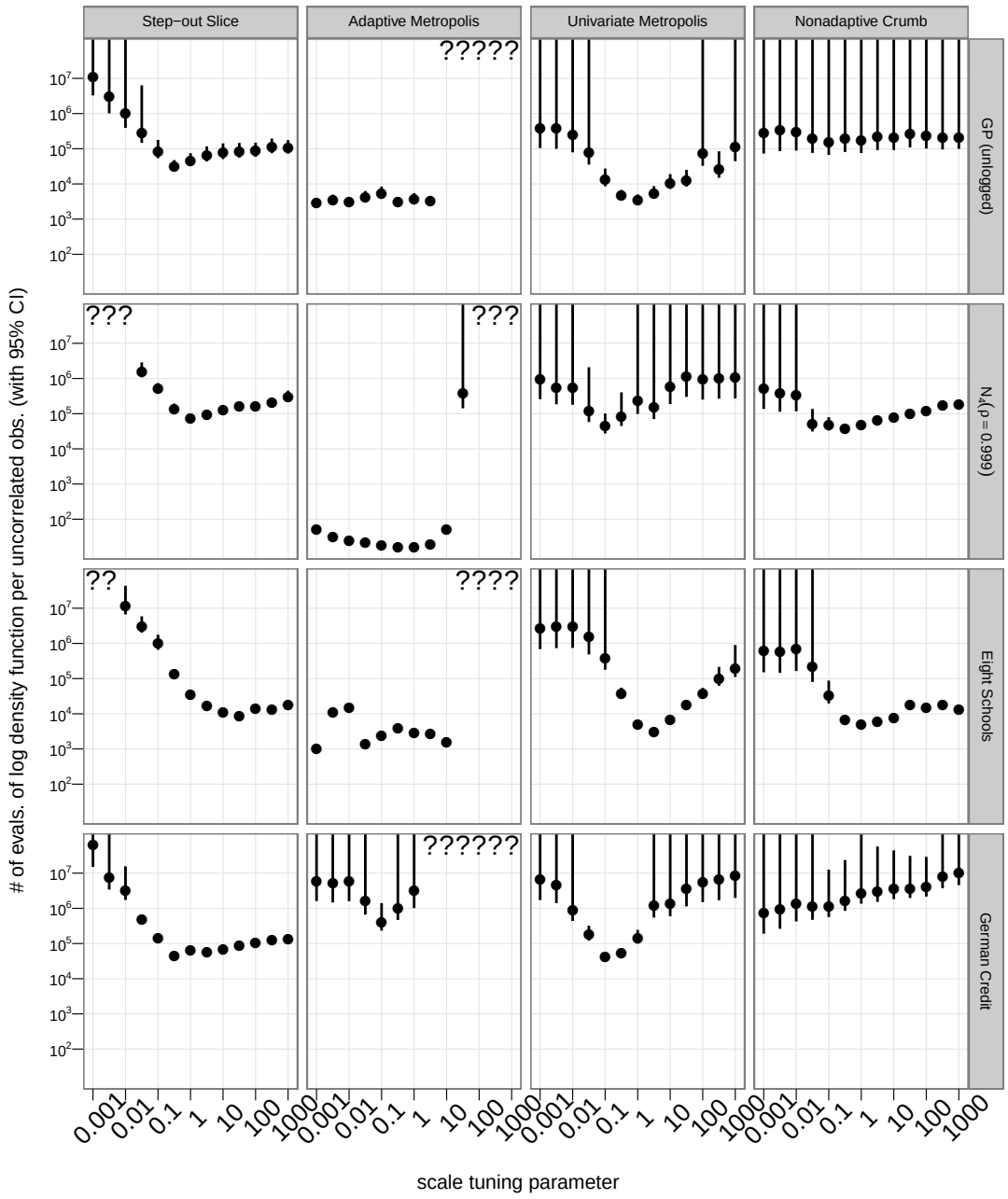

Figure 2.7: A demonstration of graphical comparison of performance of MCMC samplers. Columns of plots represent samplers; rows represent distributions. Each simulation is of length 250,000. At a glance, a researcher can see how 208 simulations relate to each other. See section 2.3 for discussion.

has a near-100% rejection rate and when Step-out Slice is badly enough tuned that the test framework aborts the simulation.

2.3.1 Between-cell comparisons

Scanning an individual cell in the grid of plots, one can see how performance varies with the tuning parameter. Scanning down columns of the grid of plots, one can see how performance varies from distribution to distribution for a given MCMC method. Scanning across rows of the grid of plots, one can see how performance varies from method to method for a given distribution.

Doing this, several patterns emerge. For example, one can see that Adaptive Metropolis performs consistently well for a variety of tuning parameters, as long as the tuning parameter is smaller than the square root of the smallest eigenvalue of the distribution's covariance. Either it performs well or does not converge at all. This suggests that Adaptive Metropolis users uncertain about the distribution they are sampling from should err in the direction of small tuning parameters.

A second pattern is that Univariate Metropolis tends to have U-shaped comparison plots. Tuning parameters that are either too small or too large lead to unacceptable performance. And, the lowest points on these plots are still usually above the flat parts of the Adaptive Metropolis plots. On low-dimensional distributions like these, where the sampler does not know the structure of the target density, Adaptive Metropolis can be considered to dominate Univariate Metropolis.

Reading across rows, one can see different sorts of patterns. For example, The GP (unlogged) and $N_4(\rho = 0.999)$ rows are flat within cells, but not between them, suggesting that for those distributions, one needs to pay more attention to the choice of method than its tuning.

2.3.2 Within-cell comparisons

A different sort of pattern can be seen in the slopes of the lines traced out by the plot symbols. For Univariate Metropolis on GP (unlogged), Eight Schools, and German Credit, for tuning parameters less than one, a decrease in the tuning parameter by a factor of ten leads to a factor of almost one hundred degraded performance—a slope of -2 in the log domain. For these tuning parameters, the Markov chains are nearly a random walk. Such a random walk will travel some distance in a number of steps proportional to the square of that distance (Feller, 1968, p. 90).

This contrasts with the slope of the plot symbols for Step-out Slice, which is close to -1 for small tuning parameters on the same distributions. Step-out Slice requires a number of log density function evaluations linear in the ratio of slice width to tuning parameter to determine an initial slice estimate, so decreasing the tuning parameter by some factor degrades the performance by that factor.

A pattern in the slopes for large parameters can be seen with Univariate Metropolis on Eight Schools with tuning parameters larger than one. In those simulations, multiplying the tuning parameter by ten degrades performance by a factor of approximately ten—a slope of one in the log domain. Increasing the tuning parameter by some factor reduces the acceptance rate by approximately that factor when the tuning parameter is large.

This behavior contrasts with the two slice samplers, whose costs trace logarithmic curves for large tuning parameters on $N_4(\rho = 0.999)$ and German Credit. On average, each rejected proposal reduces the estimated slice size by a constant factor, so an increase in a tuning parameter above the optimal value by some factor increases the computation cost by the log of that factor.

None of the patterns of this section would be easily visible if the results were presented in tabular form. Figure 2.7 shows summaries of 208 simulations, more than could be absorbed by a reader if presented as text.

2.3.3 Comparison with multiple tuning parameters

While plots like figure 2.7 allow a broad comparison of distributions and methods, it is often necessary to compare different sets of factors. The same type of plot can be used when varying extra parameters associated with either the distribution or the MCMC method. Figure 2.8 is an example of such a comparison. It focuses just on Adaptive Metropolis sampling from badly-scaled Gaussians.

One tuning parameter of Adaptive Metropolis is β, the fraction of proposals drawn from a spherical Gaussian instead of a Gaussian with a learned covariance. Roberts and Rosenthal (2009) suggest the value of 0.05. In this example, I vary it from 0.001 to 0.95.

At the same time, I consider the effect of dimensionality on the performance of the method. Each target distribution is a multivariate Gaussian with uncorrelated components. The variance is equal to 1000 in one coordinate and one in the rest. The problem dimension ranges from 2 to 128. While the high-variance component is axis-aligned, this does not affect the results because the behavior of Adaptive Metropolis is invariant to rotations of the target distribution. As with the simulations of figure 2.7, Adaptive Metropolis performs well when the principal tuning parameter is smaller than the square root of the smallest eigenvalue of the target distribution's covariance, in this case one.

Having seen this pattern, it is useful to summarize the comparisons by choosing the lowest-cost simulation from each grid cell and plotting them in a single graph, as in figure 2.9. In both figure 2.8 and figure 2.9, one can see that while Adaptive Metropolis performs better in low dimensional spaces, this performance does not vary much with β in any of the dimensions simulated.

2.3.4 Discussion of graphical comparison

Section 2.3 shows the variation in performance of MCMC methods while varying method, distribution, and one tuning parameter as well as the variation in performance of a single

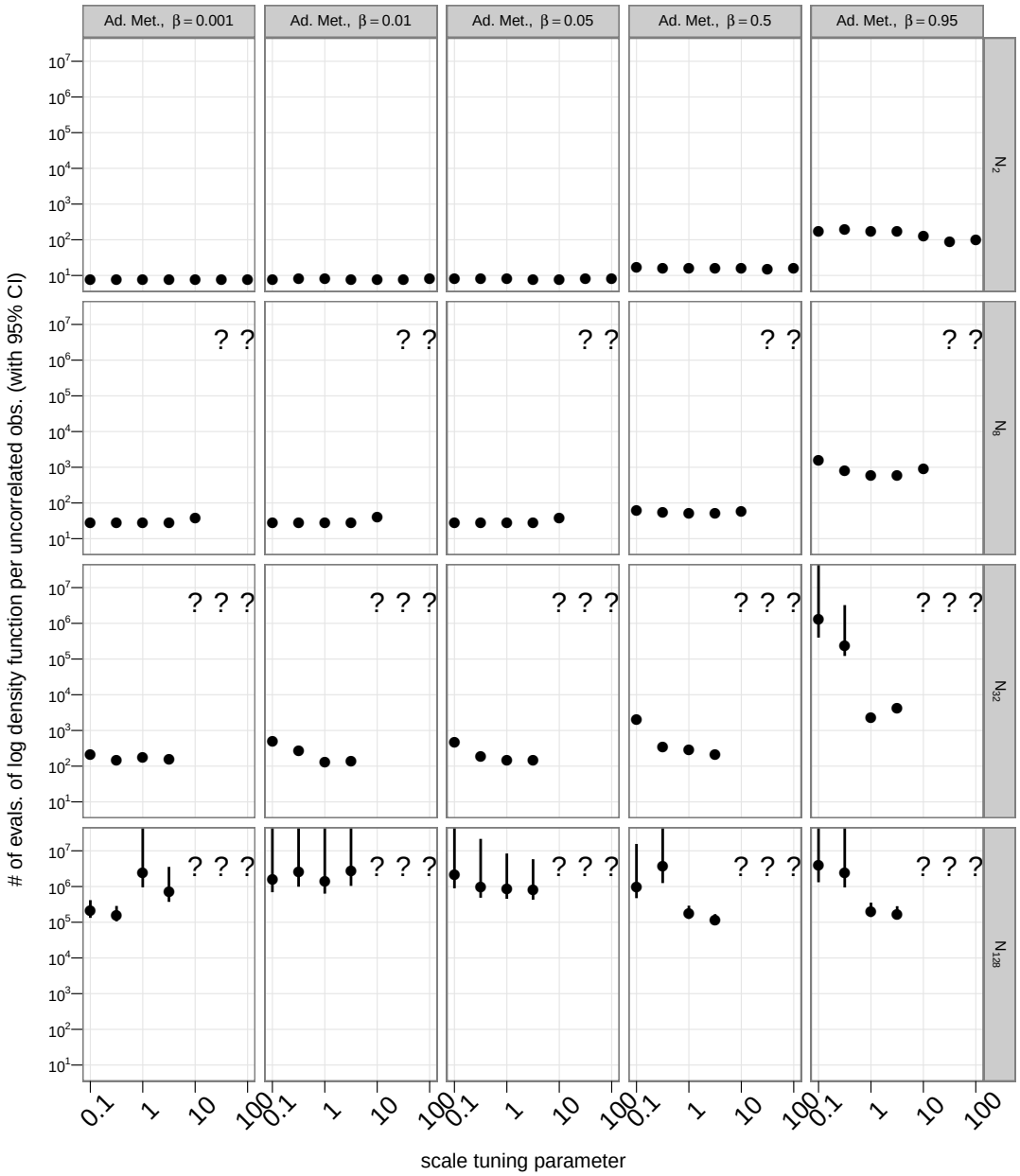

Figure 2.8: A demonstration of graphical comparison of performance of a single sampler, Adaptive Metropolis, with two tuning parameters. Columns of plots represent different values of one tuning parameter, β; the other is plotted on the horizontal axis of the subplots. Rows of plots correspond to increasing dimensions of badly-scaled Gaussian distributions. Each simulation is of length 40,000. See section 2.3.3 for discussion.

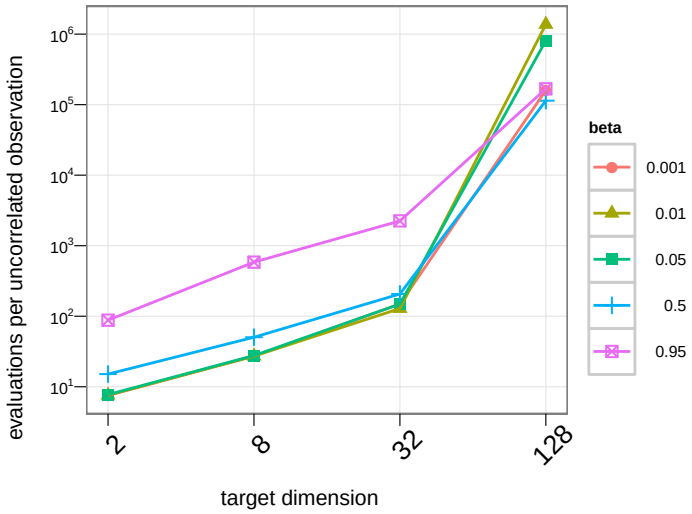

Figure 2.9: A reduced-dimension representation of figure 2.8 showing how Adaptive Metropolis scales with dimension when sampling from poorly-conditioned Gaussian distributions. Each plot symbol represents the best-performing simulation for a given dimension and value of β. See section 2.3.3 for discussion.

MCMC method while varying two tuning parameters and the dimension of the target distribution. In general, one may use the plots described in this section to compare performance of MCMC methods while varying any three factors. Comparing performance with tabulated summary statistics, in contrast, only allows researchers to study variation in one factor at once, a significant disadvantage.

One might wonder, then, how one could visualize performance as more than three factors vary simultaneously. While it may be useful, computational limits become an obstacle as the number of parameters increases. Figure 2.7 compares 208 simulations. Even if there were a clear way to visualize cost as four or five factors vary, one would need to run thousands of simulations to make such a plot. The plots of this section display approximately as much information as is currently feasible to gather.

Other variations on these plots are possible, such as the one used for figure 2.9. One variant not shown replaces confidence intervals by multiple plot symbols, each representing a replication of the same simulation with a different random seed. Multiple symbols are plotted in a column for a given tuning parameter. Making the symbols partially transparent makes such a graph easier to read.

If one is willing to forego all measures of uncertainty under replication, one can omit the confidence intervals and plot figures of merit for multiple values of a second factor, such as a second tuning parameter, in a single grid cell, differentiating levels of this factor by color or plot symbol. However, this technique can produce confusing graphs if the factor represented by color or plot symbol is not naturally nested in the factor represented by columns of plots—one should not vary a factor like problem dimension inside a single grid cell.

Chapter 3

Samplers with multivariate steps

This chapter presents several new variations of slice sampling. First, it gives background on slice sampling with multivariate steps. Then, it presents several globally-adaptive eigendecomposition-based methods and several locally-adaptive gradient-based methods in the crumb framework. Finally, it compares the methods using the scheme described in chapter 2.

3.1 Slice sampling overview

Slice sampling is a robust Markov chain Monte Carlo method in which a new state is drawn from a "slice" containing all points whose density is larger than an auxiliary variable, y. Uniformly sampling from the volume under a probability density function, $f(\cdot)$, gives a sample $\{(x_i, y_i)\}$, where $x_i \in \mathbb{R}^p$ and $y_i \in \mathbb{R}^+$. The marginal distribution of x_i then has density $f(x_i)$. So, if one can devise a way of sampling uniformly from the volume underneath a distribution's density curve, one can convert this to a method for sampling from the distribution itself by dropping the y_i from the resulting sample.

Slice sampling accomplishes this by alternating steps that update the y coordinate and steps that update the x coordinates. Updating the y coordinate is easy: the conditional distribution for y_{i+1} given x_i is uniform on the interval $[0, f(x_i)]$. Updating the

x coordinate is more difficult, in general, so instead of updating x_i with its conditional distribution, general purpose slice samplers perform a state transition that leaves the conditional distribution given y_i invariant. An update to x_i seeks an x_{i+1} such that if x_i is uniformly distributed on the current slice through the density, $\{x|f(x) \geq y_i\}$, then x_{i+1} will also be uniformly distributed on the same slice. Neal (2003) discusses various methods that satisfy this condition. This chapter and chapter 4 extend his work, focusing on adaptive multivariate updates.

The methods described in this document evaluate the log density function of the target distribution, usually denoted by $\ell(\cdot)$, rather than the density function itself, because working in the log domain makes numeric underflow and overflow less likely. Let E have an exponential distribution with mean one. The value $\exp(-E)$ has a uniform distribution, so instead of using a uniform draw on $[0, f(x)]$ as the slice level, we can use $\ell(x) - E$ as a log-domain slice level:

$$\exp(\ell(x) - E) = f(x) \cdot \exp(-E), \quad \text{where } E \sim \text{Exponential}(1) \tag{3.1}$$

$$= f(x) \cdot U, \quad \text{where } U \sim \text{Uniform}[0, 1] \tag{3.2}$$

$$\sim \text{Uniform}[0, f(x)] \tag{3.3}$$

This way, we never need to compute $\exp \ell(x)$, which can overflow or underflow.

3.2 Methods based on eigenvector decomposition

In this section, the approach to adaptive MCMC that Haario et al. (2001) use to improve random-walk Metropolis is applied to improve two variations on slice sampling. These methods continuously adapt, learning the global structure of the distribution as they move through the state space. They converge asymptotically to the target distribution, but do not have a fixed stationary distribution, so they can be difficult to analyze for convergence. They can also be difficult to embed in a larger sampling scheme because

their adapted state may become inappropriate when the variables the target distribution conditions on change.

When components of the target distribution are highly correlated, the Markov chains generated by slice samplers that make univariate updates (Neal, 2003, §4) will mix slowly. If two components are highly correlated, the contours of the target density will not be axis-aligned, so univariate slice updates with stepping out or doubling will always take steps across short, axis-aligned cuts through these contours. The hyperrectangle method (Neal, 2003, §5.1) is a slice sampling variant that takes multivariate steps by drawing proposals from an axis-aligned hyperrectangle positioned randomly with respect to the current point. It is unlikely to accept a proposal until the hyperrectangle has edges of length comparable to the shortest diameter of the log density contour that defines the current slice. Therefore, it behaves similarly to methods that take univariate updates when the components of the target distribution are highly correlated.

We must somehow take steps in non-axis-aligned directions for the Markov chain to mix quickly on distributions where components of the target distribution are highly correlated. If the target distribution is Gaussian, the contours are concentric ellipsoids. If the log density of the target distribution is convex and not highly skewed, the contours are at least roughly ellipsoidal. We can create an ellipsoidal approximation to a slice contour by aligning the axes of an ellipsoid with the eigenvectors of the sample covariance matrix and choosing the axis lengths to be proportional to the square roots of the corresponding eigenvalues. Unless the log density is unimodal and normalized, it is difficult to compute the optimal proportionality constant. (This issue is discussed in section 4.1.2.)

This idea motivates two variations on slice sampling that use an approximation to the covariance matrix of the target distribution. One approach is to take univariate steps with stepping out in the coordinate space defined by the eigenvectors, with initial slice widths proportional to the square roots of the corresponding eigenvalues. This method is discussed in section 3.2.1.

The second approach is an extension of the hyperrectangle method. The hyperrectangle method can be modified so that the axes of the initial hyperrectangles are oriented along eigenvectors, and the lengths of the sides of the initial hyperrectangle are proportional to the square roots of the eigenvalues. This method is discussed in section 3.2.3.

Both methods require an approximation of the covariance matrix. Haario et al. (2001) show that one can use a mixture of spherically symmetric Gaussian proposals and the sample covariance matrix to generate an adaptive Metropolis proposal distribution. Using a theorem from Roberts and Rosenthal (2007), they show that the resulting Markov chain converges to the intended distribution. Section 3.2.5 uses a similar argument to show that the modified hyperrectangle method converges to the intended distribution.

3.2.1 Univariate updates along eigenvectors

"Univar Eigen," inspired by Tibbits et al. (2010), is a variation of slice sampling that makes univariate updates along the eigenvectors of the sample covariance matrix. If the log density of the target distribution is approximately convex, so that there is not radical variation in the shape of the target distribution from point to point, the contours of the distribution will be approximately ellipsoidal and the eigenvectors of its covariance will roughly coincide with the axes of these ellipsoids. Steps taken along the eigenvectors, therefore, will include steps along the long axes of a slice even when the axes of the contours do not coincide with the coordinate axes.

Computing these directions requires an estimate of the covariance. Tibbits et al. use the sample covariance from a trial run to estimate the full covariance matrix of the hyperparameters and the marginal variances of the remaining parameters. Univar Eigen instead uses the full sample covariance matrix of the current chain, as done by Haario et al. (2001) in Adaptive Metropolis. Like Adaptive Metropolis, Univar Eigen takes a small fraction of its steps from a fixed distribution to avoid becoming trapped in a bad adaptive state. It has two tuning parameters: β, the proportion of iterations that use

non-adapted steps, and w, the initial segment length for non-adapted steps. β is usually fixed at 0.05, as in Adaptive Metropolis.

Suppose our Markov chain has taken n steps, generating a sequence of dependent p-vector-valued random variables $(X_1, \ldots, X_n)$ from the target distribution. Denote the sample covariance of this sequence by S_n. Denote the eigenvectors of S_n by $(v_1, \ldots, v_p)$ and the eigenvalues of S_n by $(\lambda_1, \ldots, \lambda_p)$. Each iteration, Univar Eigen chooses a random number $U \in [0, 1]$. If $U < \beta$ or $n < p$ (making S_n rank-deficient), the initial slice approximation is a segment of length w in a random direction placed so that the offset of the current state, X_n, from the end of the segment is uniformly distributed on $[0, w]$. If $U \geq \beta$, an eigenvector-eigenvalue pair (v_i, λ_i) is chosen, with i uniformly drawn from $\{1, \ldots, p\}$. The initial slice proposal is then a segment of length $\sqrt{\lambda_i}$ in the direction v_i placed so that the offset of the current state from the end of the segment is uniformly distributed on $\left[0, \sqrt{\lambda_i}\right]$.

The initial segment can be expanded by stepping out as discussed in Neal (2003, §4), but this is not strictly necessary since using an eigenvalue to compute the initial slice approximation leads to reasonable scaling. However, stepping out does lead to greater robustness and has minimal downside. It is used in the experiments of section 3.2.2, but the results are similar if it is not. Once an initial slice approximation is chosen, a proposal for X_{n+1} is drawn uniformly from the segment. If the proposed step is outside the slice, it is rejected and the segment is shrunk so that the next proposal is drawn from the portion of the segment on the same side of the rejected proposal as X_n. Proposals are drawn and the approximation shrunk until a proposal is accepted.

When the target distribution is p-dimensional, the computation of the eigendecomposition of S_n is $O(p^3)$, so it is not done every iteration. In the implementation evaluated here, the number of decomposition updates is limited to one hundred. For example, on a chain length of 50,000, the eigendecomposition will be updated every 500 iterations. Only one in every p univariate updates is used to update the scatter matrix used to compute

S_n, and each update takes $O(p^2)$ operations. Since an individual one-dimensional update takes $O(p)$ operations, neither the cost of updating the eigendecomposition nor the cost of maintaining the scatter matrix is dominant for long chains or in high-dimensional spaces.

3.2.2 Evaluation of univariate updates

Univar Eigen learns a covariance matrix like Adaptive Metropolis (Haario et al., 2001) and takes steps of the type used by slice sampling with stepping out (Neal, 2003, §4). Figure 3.1 shows the results of a comparison of these three methods using the four test distributions described in section 2.2.2 using the plots described in section 2.3. In addition, it includes a variation, "Cheat Univar Eigen," that uses the true covariance instead of the adaptive estimate used by Univar Eigen. The true covariance is unknown for real problems, but including this variant distinguishes performance characteristics of the underlying method from performance differences related to inadequate covariance estimates. The scale tuning parameter for Univar Eigen and Cheat Univar Eigen is the initial slice approximation length for the non-adaptive steps, w; β is set to 0.05 for both. Simulations generated by Univar Eigen are nonstationary, so autocorrelation-time based cost measures are not strictly appropriate. However, these simulations are long enough that the simulations are approximately stationary. It can be seen in figure 3.1 that Univar Eigen and Cheat Univar Eigen perform similarly in all the chains simulated, suggesting that the covariance estimator used by Univar Eigen is adequate.

While Adaptive Metropolis sometimes has a moderate edge on Univar Eigen when carefully tuned, Univar Eigen generally performs as well or better than either of the two methods on which it is based. The difference is particularly striking on the German Credit distribution. Univar Eigen and Cheat Univar Eigen perform similarly, and both are substantially better than Adaptive Metropolis and Step-out Slice. This shows that both the ability to take large steps using the learned global structure and the ability to

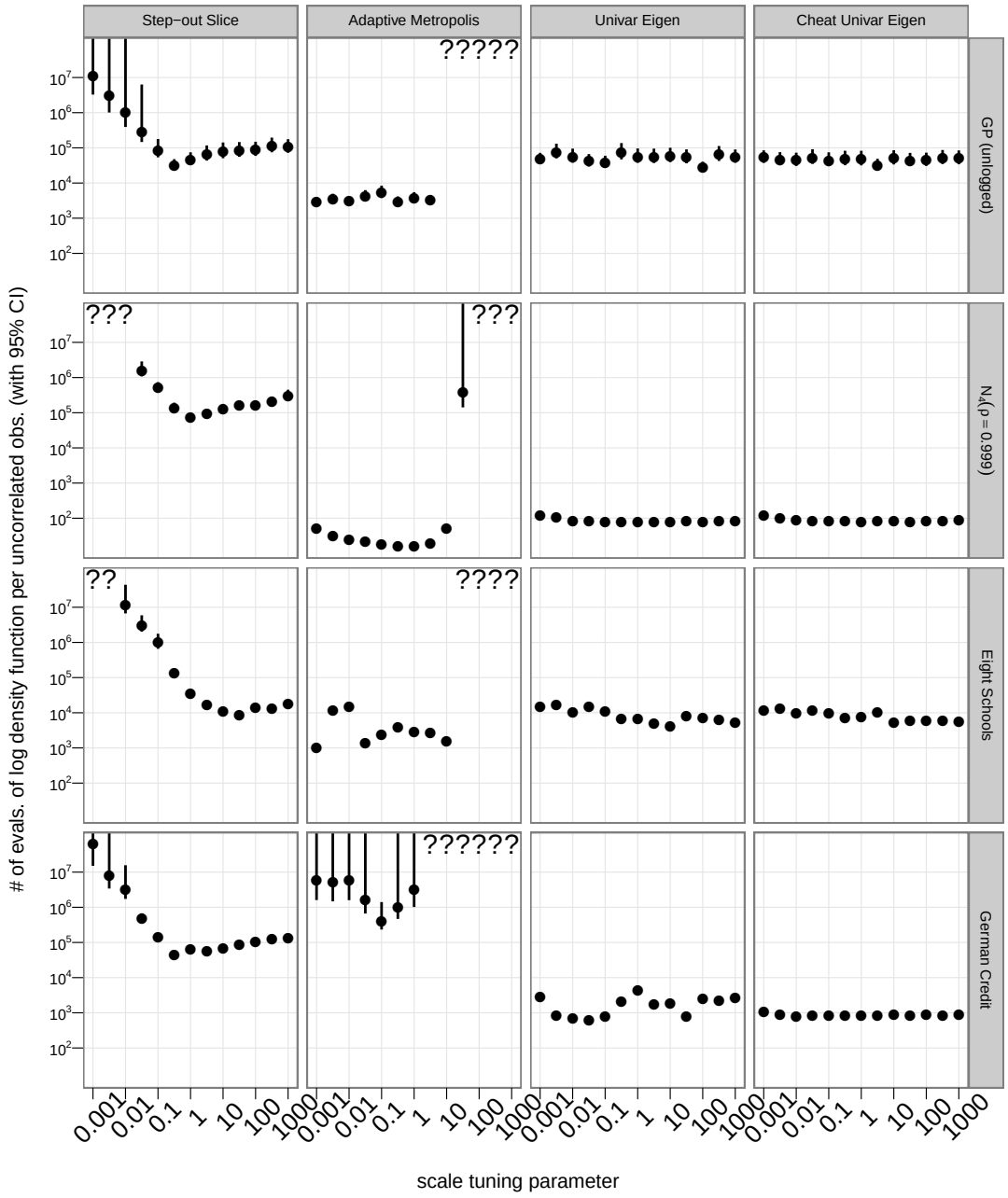

Figure 3.1: A comparison of Univar Eigen to two other MCMC methods using simulations of length 50,000. Question marks indicate simulations that were aborted or trapped in a single state. See section 3.2.2 for discussion.

take small steps when the local structure differs from the global structure contribute to fast mixing.

Because of the promise shown by Univar Eigen in this section, it is included in a broader comparison of methods in section 3.6.

3.2.3 Multivariate updates with oblique hyperrectangles

Section 3.2.1 extends slice sampling with stepping out to use a coordinate system based on the covariance of the target distribution; this section similarly extends the hyperrectangle method (Neal, 2003, §5.1), which takes multivariate steps in a slice using a hyperrectangular initial slice approximation.

In each iteration of Neal's hyperrectangle method, an axis-aligned hypercube approximating the slice is placed randomly so that the distribution of the current state is uniform relative to the hypercube. A proposal is then drawn from the hypercube; if it is inside the slice, it is accepted. Since the distributions of the current state and the proposal are the same relative to the hypercube, the stationary distribution is invariant. If the proposal is not in the slice, just as a segment is shrunk towards the current state when sampling with univariate updates, the hypercube is divided in two by the hyperplane through the rejected proposal and normal to the coordinate direction in which the gradient of the log density is largest, and the section of the hypercube not containing the current state is removed from the approximation. Then, a new proposal is drawn, a new section of the hyperrectangle is removed if this proposal is not in the slice, and so on until a proposal is inside the slice. If gradients are not available, instead of only shrinking one coordinate, every coordinate is shrunk towards the initial state, leaving the rejected proposal as a corner of the updated hyperrectangular slice approximation. (Figure 3.3 on page 45 includes a graphical example of these updates.)

If gradients are available, efficient sampling is possible on distributions whose components have greatly unequal variances but little correlation. If gradients are not available,

efficient sampling is only possible on distributions whose coordinates are uncorrelated and have similar variances because a proposal will only be accepted when the slice approximation has edge sizes comparable to the least variable coordinate.

Here, I present an alternative hyperrectangle method that uses an approach similar to that of section 3.2.1. It orients the initial hyperrectangle so that its edges are parallel to the eigenvectors of the sample covariance and have lengths proportional to the square roots of the eigenvalues of the sample covariance. Since the approximation is hopefully properly scaled and aligned with the contours, when a proposal is rejected, it is reasonable to assume that the estimate is too large in all directions and that gradients are not necessary to pick a direction in which to shrink the approximation.

This method has two tuning parameters, β and w, similar to the parameters with the same names in section 3.2.1. An iteration begins by creating an initial hyperrectangular slice approximation. With probability β, the initial hyperrectangle is a unit hypercube with edge length $5w$ and axes aligned with the coordinate axes. Otherwise, axis i (for $i \in (1, \ldots, p)$) has length $5\sqrt{\lambda_i}$ and orientation v_i. In either case, the hyperrectangle is positioned so that the offset of the current state, X_n, from a corner of the initial hyperrectangle has a uniform distribution.

A proposal is drawn uniformly from the hyperrectangle, and the log density at the proposal is evaluated. If the log density is greater than or equal to the slice level, the proposal is accepted. Otherwise, it is rejected, and the hyperrectangle is shrunk without changing the orientation of its axes so that the rejected proposal is a corner of the hyperrectangular slice approximation and the current state remains in the interior of the hyperrectangle. Proposals are drawn, and the slice approximation is shrunk, until a proposal is accepted. This procedure is identical to the procedure described by Neal except in the way that the initial hyperrectangle is chosen.

Empirically, the performance of the method does not depend much on the proportionality constant for the edge lengths, five. If the constant is at least one, the slice

approximation will be larger than a typical slice, and the hyperrectangle volume will decrease exponentially as proposals are rejected. So, excessively large values degrade performance only slightly, much like excessively large tuning parameters degrade the performance of the standard hyperrectangle method only slightly, as seen in figure 3.2 on page 41.

3.2.4 Evaluation of hyperrectangle updates

Just as Univar Eigen is a fusion of slice sampling with stepping out and Adaptive Metropolis, the oblique hyperrectangle method is a fusion of the hyperrectangle method and Adaptive Metropolis. So, this section compares the oblique hyperrectangle method to Adaptive Metropolis and the hyperrectangle method, both with and without gradients. As with Univar Eigen, a "cheat" version of the sampler that takes the target distribution's covariance as a given instead of learning it from prior states is included for comparison.

The results of this comparison are shown in figure 3.2, a plot of the cost of an uncorrelated observation against a scale tuning parameter for each sampler and distribution. For the hyperrectangle methods, the scale tuning parameter is w, the edge length of the initial hypercube. The oblique hyperrectangle methods perform similarly to or better than Adaptive Metropolis and the standard hyperrectangle variants at their best for nearly all values of w. That is, the performance of the oblique hyperrectangle method is similar to the reference methods when all methods' tuning parameters are well-chosen, but outperforms the others when they are not.

As with Univar Eigen, the performance of Cheat Oblique Hyperrect and that of Oblique Hyperrect are similar, though an exception occurs on German Credit. Its dimension is 25, more than the other three, so the covariance has 325 free parameters. They are not estimated well by either Oblique Hyperrect or Adaptive Metropolis by a simulation of length 50,000. A risk of using MCMC methods that converge but are not

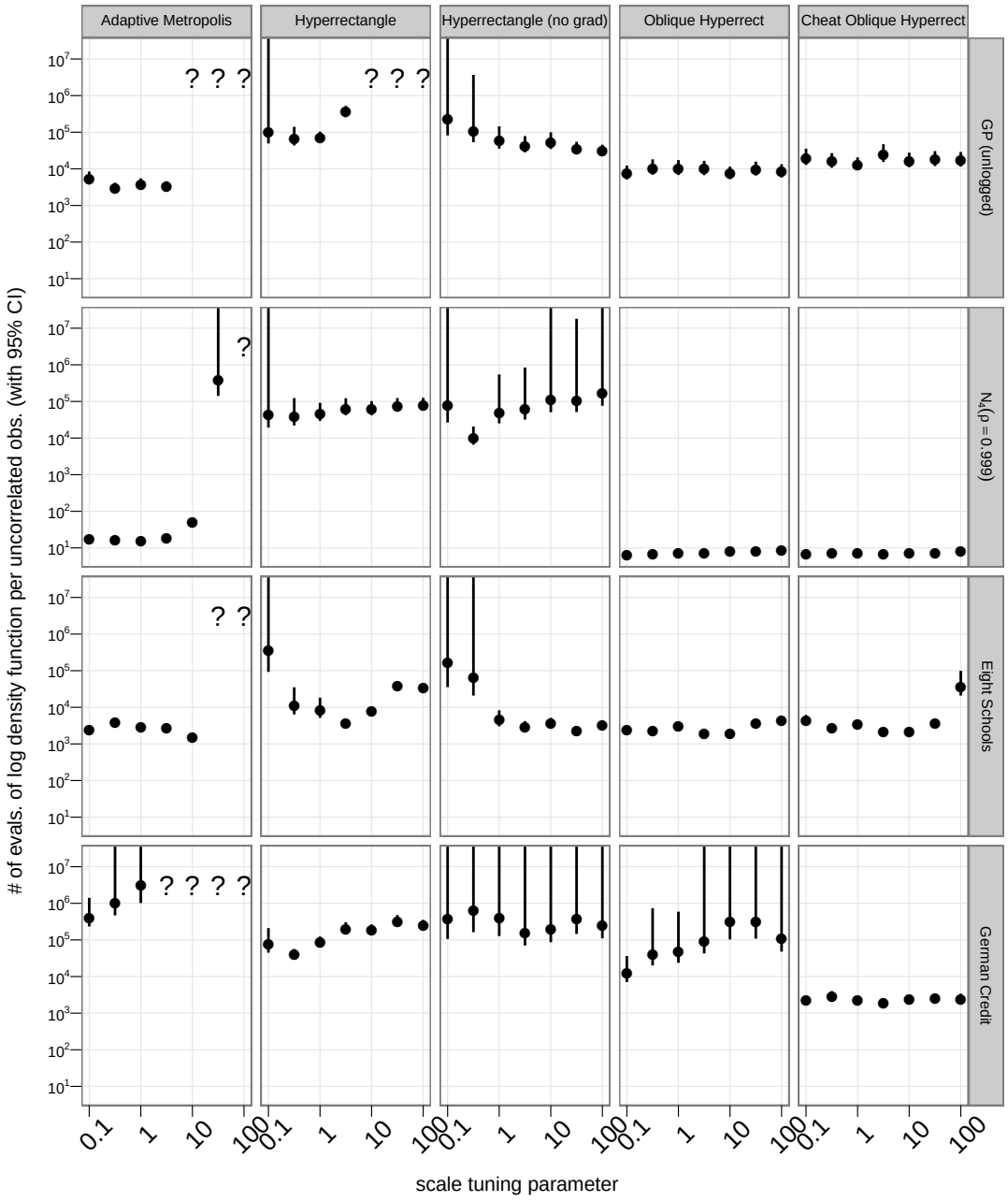

Figure 3.2: A comparison of oblique hyperrectangle slice sampling to Adaptive Metropolis and the two standard variants of the hyperrectangle method using simulations of length 50,000. Question marks are plotted for simulations that were aborted or trapped in a single state. See section 3.2.4 for discussion.

stationary is that diagnostic summaries are dependent on the simulation length.

Like Univar Eigen, Oblique Hyperrect shows potential and is included in a broader comparison of methods in section 3.6.

3.2.5 Convergence of the oblique hyperrectangle method

In this section, I use a theorem of Roberts and Rosenthal to show that the distribution of the observations generated by the oblique hyperrectangle method converges to the target distribution in the total variation norm as a consequence of its diminishing adaptation when it is used to sample from distributions with connected, compact support. The support of the target distribution must be connected because otherwise, even the non-adaptive hyperrectangle method might not converge to the target distribution.

Roberts and Rosenthal (2007) show that several sets of conditions are sufficient for an adaptive MCMC method to converge to the target distribution. All of these conditions include "diminishing adaptation," defined as:

$$\sup_x \|P_{\Gamma_{n+1}}(x,\cdot) - P_{\Gamma_n}(x,\cdot)\|_{\mathrm{TV}} \to 0 \quad \text{in probability as } n \to \infty \tag{3.4}$$

Here, $P_{\Gamma_n}(x,\cdot)$ is the transition density at iteration n with "adaptation state" Γ_n and current state x. The norm, $\|\cdot\|_{\mathrm{TV}}$, is the total variation norm. For the oblique hyperrectangle method, the adaptation state is the sample covariance, which encapsulates all non-constant aspects of the transition density at a particular iteration.

When computing the sample covariance matrix, each iteration has weight $1/n$. Since oblique hyperrectangle transitions are bounded by the initial hyperrectangle, the most extreme transition can only move a finite distance from the center of the hyperrectangle. The relative change in the ith eigenvalue between steps n and $n+1$ is $O(1/n)$ since the maximum step size in the direction of the corresponding eigenvector is proportional to the square root of that eigenvalue. The same holds for updates to the eigenvectors: the eigenvectors of Γ_{n+1} are a mixture of the eigenvectors of Γ_n and the observation at

iteration n, where the total weight given to the observation at iteration n over all the directions is $O(1/n)$. Since each eigenvalue can change by $O(1/n)$ and each eigenvector can rotate by an angle $O(1/n)$, each initial hyperrectangle diameter can change by $O\big(1/\sqrt{n}\big)$. Conditioning on the random draw that positions the initial hyperrectangles with respect to the current state, the ratio of the volume occupied by the symmetric difference between the hyperrectangles for states Γ_n and Γ_{n+1} to the volume of either hyperrectangle is $O\big(1/\sqrt{n}\big)$. Therefore, the probability of a proposal falling inside one hyperrectangle and not another is $O\big(1/\sqrt{n}\big)$; the difference in densities for proposals falling inside both is also $O\big(1/\sqrt{n}\big)$. Consequently, the total variation distance between $P_{\Gamma_n}(x,\cdot)$ and $P_{\Gamma_{n+1}}(x,\cdot)$ is $O\big(1/\sqrt{n}\big)$, where the proportionality constant does not depend on x, so the diminishing adaptation condition is satisfied. Golub and Van Loan (1996, pp. 395–397) discuss changes in eigendecompositions after rank-one updates in greater detail.

If the target distribution has compact, connected support, the non-adaptive hyperrectangle method converges to the target distribution for any initial state and any full-rank initial hyperrectangle orientation and dimensions. Let the space of adaptive states be the set of all positive definite covariance matrices with all eigenvalues no smaller than some positive lower bound. Because the maximum eigenvalue of the covariance matrices is limited by the the boundedness of the support of the target distribution, this space is compact with respect to the Euclidean norm. The probability mass in the difference between two full-rank initial hyperrectangles in a neighborhood of γ will shrink to zero as the size of the neighborhood approaches zero, so the mapping $(x,\gamma) \mapsto P_\gamma(x,\cdot)$ is continuous with respect to the total variation norm. By lemma 1 of Roberts and Rosenthal (2007), this implies that the mapping $(x,\gamma) \mapsto \|P_\gamma^n(x,\cdot) - f(\cdot)\|_{\mathrm{TV}}$ is also continuous. This continuity, along with diminishing adaptation and the convergence of $P_\gamma^n(x,\cdot)$ to $f(\cdot)$ for each individual x and γ, imply, by corollary 3 of Roberts and Rosenthal (2007), that the adaptive hyperrectangle method converges to the target distribution in total

variation.

An immediate consequence is that the expectation of all bounded functions of state of the Markov chain converge to their expectations with respect to the target distribution. Since this applies at every point in the chain, the sample mean of a bounded function of state is an asymptotically unbiased estimator of the expectation of that function with respect to the target distribution.

The argument of this section cannot be directly used to show that Univar Eigen converges to the target distribution. Univar Eigen only takes steps along eigenvectors, so a proof of convergence would need to consider multiple steps along eigenvectors as a group to demonstrate diminishing adaptation.

3.3 Irregular polyhedral slice approximations

Section 3.2.3 extended the hyperrectangle method by allowing the orientation of the hyperrectangular slice approximation to depend adaptively on global state. This section describes an alternative that, instead of reorienting the initial hyperrectangle, allows it to deform into non-hyperrectangular polyhedra. Assume the gradient of the log density is available. When a proposal is rejected, instead of dividing the slice approximation by a hyperplane normal to the gradient's largest coordinate and updating the approximation to be the portion of the approximation on the same side as the current point, divide the approximation by a hyperplane normal to the gradient itself. The approximation can then shrink quickly to approximate any convex shape. This technique is illustrated for a two-dimensional slice in figure 3.3.

Unfortunately, after the first rejection, the slice approximation is irregular, and sampling uniformly from an irregular polyhedron is difficult. One approach to this subproblem is rejection sampling. It is straightforward to compute the minimum bounding hyperrectangle for a convex body defined by a set of hyperplanes. Unfortunately, since the

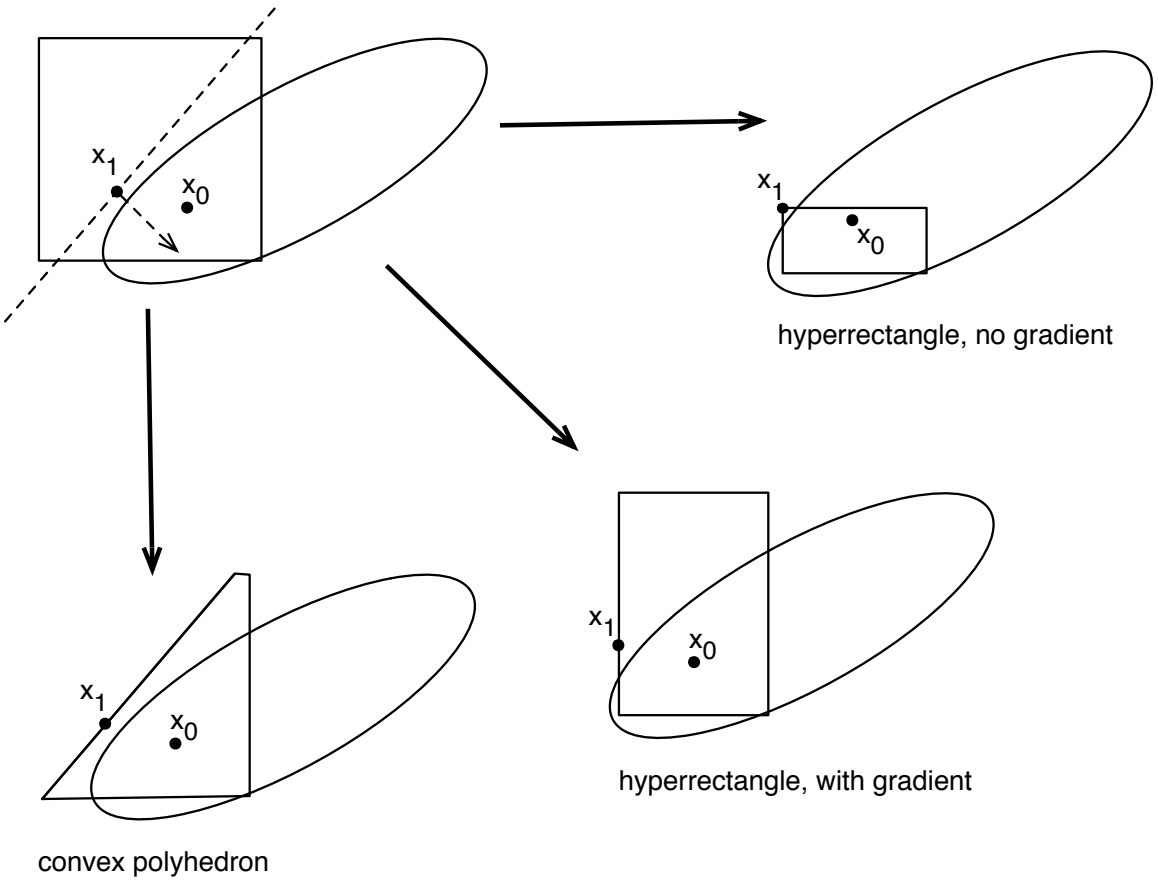

Figure 3.3: Three different ways to update a hyperrectangular slice approximation. The true slice is shown as an ellipse, the approximation is shown as a polygon, and the initial state is marked x_0. (Upper left) A hyperrectangular approximation of the slice is drawn, and a proposal, x_1, is drawn from the approximation. It is outside the slice, so it is rejected. The gradient at x_1 is shown as a dashed arrow; the hyperplane normal to the gradient is shown as a dashed line. (Upper right) In the standard hyperrectangle method without gradients, the approximation is shrunk so that x_1 is a corner of the updated approximation. (Lower right) In the standard hyperrectangle method with gradients, the approximation is shrunk toward x_0 in the direction where the gradient at x_1 is the largest, so that x_1 lies on a face of the updated approximation. (Lower left) If approximations can be convex polyhedra, a new face normal to the gradient at x_1 is added to the approximation.

motivation for allowing polyhedral slice approximations is that hyperrectangles are not a tight enough approximation to a slice, this method is infeasible—in high-dimensional spaces, vanishingly few candidate proposals drawn from a bounding hyperrectangle are inside the polyhedral slice approximation.

Alternatively, instead of rejection sampling from a bounding hyperrectangle, one could sample from a bounding ellipsoid with axes not aligned with the coordinate axes. Finding a minimum-volume ellipsoid containing a convex polyhedron is a convex optimization problem and can be expressed as a semidefinite program (Boyd and Vandenberghe, 2004, pp. 169–170). The fastest known way to solve such problems is the barrier method (Boyd and Vandenberghe, 2004, pp. 261–278), which must estimate $O(p^2)$ parameters each iteration of the Markov chain, and so is prohibitively slow.

A simpler approach is to update the bounding ellipsoid from the previous proposal instead of finding a new one each time. Given a bounding ellipsoid for proposal k and a hyperplane normal to the gradient at the rejected proposal, the bounding ellipsoid for the slice approximation for proposal $k + 1$ would be the minimum volume ellipsoid that contains all of the points of the ellipsoid on the same side of the hyperplane as the current point. This is a well-studied problem; it is at the heart of the ellipsoid method for linear programming (Grötschel et al., 1993, ch. 3). Unfortunately, the available solutions are not satisfactory. The expected volume reduction in the ellipsoid is exponentially decreasing in its dimension. Even though the polyhedron that the ellipsoid approximates shrinks in volume by a factor independent of dimension on a typical iteration, the bounding ellipsoid itself shrinks much more slowly. Rejection sampling based on the ellipsoidal approximation takes unacceptably long if the target distribution has more than a few dimensions (empirically, around four).

The fundamental problem with this approach is that arbitrarily shaped convex polyhedra are difficult to sample from. Sections 3.4 and 3.5 address this issue by approximating the slice with a Gaussian distribution instead of a uniform distribution. Since the family

of Gaussian distributions is conjugate to itself, the proposal distribution conditional on rejected points remains simple. Yet, it is still possible to derive such a slice approximation entirely from information obtained in a single MCMC iteration, as with the polyhedral method described in this section.

3.4 Covariance matching

Sections 3.2 and 3.3 describe methods for taking multivariate steps using uniform proposal distributions. This section takes an alternate approach, using Gaussian proposal distributions in the crumb framework (Neal, 2003, §5.2). Each sampler iteration in the crumb framework, a crumb is drawn, and a proposal is drawn from the distribution of initial states that could have generated that crumb. If the proposal is in the slice, it is accepted. Otherwise, a second crumb is drawn, a second proposal is drawn from the distribution of possible initial states conditional on having drawn both crumbs, and so on until a proposal is accepted.

Crumb distributions may depend on, amongst other things, the log density and gradient at rejected proposals. This section describes one way to choose the crumb distributions to reduce autocorrelation times on badly scaled distributions with correlated parameters. The method attempts to match the proposal distribution to the local curvature of the log density. It assumes that while computing the log density at a proposal, one can compute its gradient with minimal additional cost. This is often a realistic assumption, since the log density and its gradient are often computed from the same intermediate values. The human effort required to implement the gradient function is almost always more relevant.

3.4.1 Adaptive Gaussian crumbs

Let $\ell(\cdot)$ be the log density of the target distribution, let y_{slice} be the current slice log density, and let S be the slice through the distribution at that level:

$$S = \{x | \ell(x) \geq y_{\text{slice}}\} \tag{3.5}$$

Ideally, the proposal distribution would be a uniform distribution over S. To approximate uniform sampling over S, we draw a sequence of crumbs that produces a Gaussian proposal distribution with the same covariance matrix as a uniform distribution over S.

Since there are no rejected proposals to adapt on when the first crumb is drawn, the first crumb has a fixed multivariate Gaussian distribution:

$$c_1 \sim N(x_0, W_1^{-1}) \quad \text{where } W_1 = \sigma_c^{-2} I \tag{3.6}$$

The standard deviation of the initial crumb, σ_c, is the only tuning parameter for this method that is modified in normal use; it is reasonable to set it to a guess of the largest marginal standard deviation of the components of the target distribution divided by the square root of the distribution's dimension, as with equation 4.10. Larger values degrade performance only slightly, so it is better to err on the high side.

The distribution for x_0 given c_1 is a Gaussian with mean c_1 and precision matrix W_1, so we draw a proposal from this distribution:

$$x_1 \sim N(c_1, W_1^{-1}) \tag{3.7}$$

If $\ell(x_1)$ is at least y_{slice}, then x_1 is inside S, so we accept x_1 as the next state of the chain.

When a proposal, x_k, is not in the slice, we choose a different precision matrix, W_{k+1}, for the next crumb, so that the covariance of the next proposal will look more like that of uniform sampling over S. After sampling k crumbs from Gaussians with mean x_0 and precision matrices $(W_1, \ldots, W_k)$, the distribution for the kth proposal (the posterior for

x_0 given the crumbs) is:

$$x_k \sim N(\bar{c}_k, \Lambda_k^{-1}) \tag{3.8}$$

$$\text{where } \Lambda_k = W_1 + \cdots + W_k \tag{3.9}$$

$$\text{and } \bar{c}_k = \Lambda_k^{-1}(W_1 c_1 + \cdots + W_k c_k) \tag{3.10}$$

The posterior precision is the sum of the precisions of the crumbs; the posterior mean is the sample mean of the crumbs, weighted by their precisions. If $\ell(x_k)$ is at least y_{slice}, x_k is accepted as the next state. Otherwise, we must choose a covariance for the distribution of $(k+1)$th crumb, draw a new proposal, and repeat until a proposal is accepted.

3.4.2 Adapting the crumb covariance

This section describes a particular method for choosing a precision matrix, W_{k+1}, for the $(k+1)$th crumb, so that the covariance of the next proposal will approximate that of uniform sampling over S. Specifically, it attempts to find W_{k+1} so that the $(k+1)$th proposal distribution has the same conditional variance as uniform sampling from S in the direction of the gradient of $\ell(\cdot)$ at x_k. This gradient is a good guess at the direction in which the proposal distribution is least like S; figure 3.4(a) illustrates this. With a two-dimensional Gaussian target distribution (with correlation equal to 0.95), I drew a crumb with σ_c equal to one and plotted the gradients of the log density at several points drawn from the resulting proposal distribution. Most of these gradients point in the direction where the spherically-symmetric proposal variance is least like the slice. Usually, in an ill-conditioned distribution, gradients at rejected proposals do not point towards a mode, they point towards the nearest point on the slice. (In a well-conditioned distribution, the directions to a mode and to the nearest point on the slice will be similar.)

To compute W_{k+1}, we estimate the second derivative of the target distribution in the direction of the gradient, assuming the target distribution is approximately locally Gaussian. Consider the (approximately) parabolic cut through the log-density surface

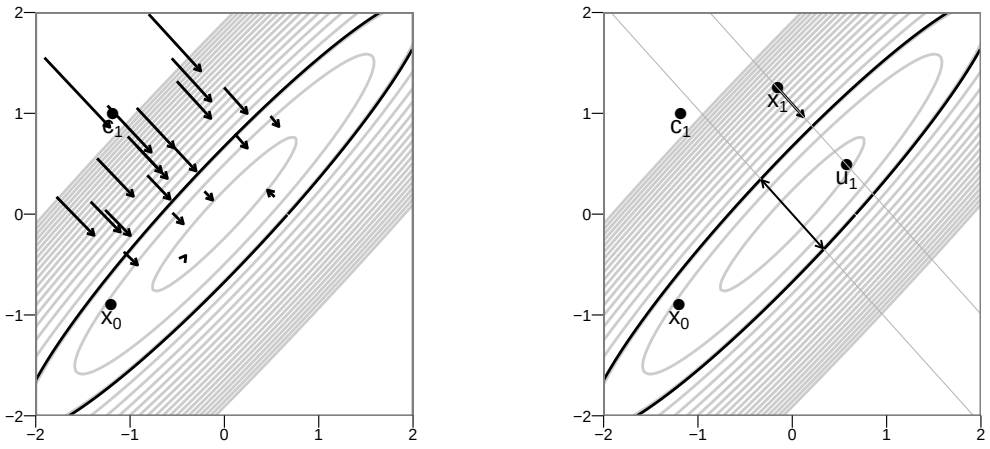

(a) (b)

Figure 3.4: (a) shows contours of the target distribution as thin grey ellipses and shows gradients at several points drawn from the first proposal distribution, a Gaussian centered at c_1. These gradients tend to point towards the slice, shown as a thick black ellipse. (b) shows two parabolic cuts through the log-density surface in the direction of the gradient at a rejected proposal, x_1. One cut passes through x_1; the other passes through the mode. The gradient at x_1 is shown as an arrow. u_1 is a point on the cut through x_1 defined by equation 3.16. The two parabolas have approximately the same second derivative. The distance between the two arms of the second parabola when the vertical coordinate is equal to y_{slice} is shown as a double-ended arrow, equal to d in equation 3.20.

passing through x_1 in figure 3.4(b). This cut has the equation:

$$\tilde{\ell}_1(t) = -\frac{1}{2}\kappa t^2 + \beta t + \gamma \tag{3.11}$$

t is a parameter that is zero at the rejected proposal and increases in the direction of the gradient; κ, β, and γ are unknown constants we wish to estimate. The coefficient $-\frac{1}{2}$ is arbitrary; this choice makes κ equal to the negative of the second derivative of the parabola. We already had to compute $\ell(x_k)$ to determine whether x_k was in S; we assume that $\nabla\ell(x_k)$ was computed simultaneously. To fix two degrees of freedom of the parabola, we plug these quantities into equation 3.11 and its derivative with respect to t:

$$\ell(x_k) = -\frac{1}{2}\kappa \cdot 0^2 + \beta \cdot 0 + \gamma = \gamma \tag{3.12}$$

$$\|\nabla\ell(x_k)\| = -\kappa \cdot 0 + \beta = \beta \tag{3.13}$$

There is still one degree of freedom remaining, so we must evaluate $\ell(\cdot)$ at another point on the parabola. We choose a point as far away from x_k as c_k is, hoping that this distance is within the range where the distribution is approximately Gaussian. Let δ be this distance:

$$\delta = \|x_k - c_k\| \tag{3.14}$$

Let g be the normalized gradient at x_k:

$$g = \frac{\nabla\ell(x_k)}{\|\nabla\ell(x_k)\|} \tag{3.15}$$

Then, the point u_k is defined to be δ away from x_k in the direction g:

$$u_k = x_k + \delta \cdot g \tag{3.16}$$

In equation 3.11, u_k corresponds to $t = \delta$. We evaluate the log density at u_k to fix the parabolic cut's third degree of freedom, and plug this into equation 3.11:

$$\ell(u_k) = -\frac{1}{2}\kappa\delta^2 + \beta\delta + \gamma \tag{3.17}$$

Solving equations 3.12, 3.13, and 3.17 for κ gives:

$$\kappa = -\frac{2}{\delta^2}\big(\ell(u_k) - \ell(x_k) - \|\nabla\ell(x_k)\| \cdot \delta\big) \tag{3.18}$$

We can now use κ to approximate the conditional variance in the direction g. If the Hessian is locally approximately constant, as it is for Gaussians, a cut through the mode in the direction of $\nabla\ell(x_k)$ would have the same second derivative as the cut through x_k. This second parabola, also shown in figure 3.4(b), has the equation:

$$\tilde{\ell}_2(t) = -\frac{1}{2}\kappa t^2 + M \tag{3.19}$$

M is the log density at the mode. We set $t = 0$ at the mode, so there is no linear term. For now, assume $\ell(\cdot)$ is unimodal and that M was computed with the conjugate gradient method (Nocedal and Wright, 2006, ch. 5) or some other similar procedure before starting the Markov chain. We solve equation 3.19 for the parabola's diameter d at the level of the current slice, y_{slice}, shown as a doubled-ended arrow in figure 3.4(b):

$$d = \sqrt{\frac{8(M - y_{\text{slice}})}{\kappa}} \tag{3.20}$$

Since the distribution of points drawn from an ellipsoidal slice, conditional on their lying on that particular one-dimensional cut, is uniform with length d, the conditional variance in the direction of the gradient at x_k is:

$$\sigma^2_{k+1} = \frac{d^2}{12} = \frac{2}{3} \cdot \frac{M - y_{\text{slice}}}{\kappa} \tag{3.21}$$

With this variance, we can construct a crumb precision matrix that will lead to the desired proposal precision matrix. We want to draw a crumb c_{k+1} so that the posterior of x_0 given the k crumbs has a variance equal to σ^2_{k+1} in the direction g. Equation 3.9 indicates that the precision of the proposal given these crumbs is:

$$\Lambda_{k+1} = \Lambda_k + W_{k+1} \tag{3.22}$$

If we multiply both sides of equation 3.22 by g^T on the left and g on the right, the left side is the conditional precision in the direction g.

$$g^T \Lambda_{k+1} g = g^T \big(\Lambda_k + W_{k+1}\big) g \tag{3.23}$$

We would like to choose W_{k+1} so that this conditional precision is σ_{k+1}^{-2}, so we replace the left hand side of equation 3.23 with that:

$$\sigma_{k+1}^{-2} = g^T \big(\Lambda_k + W_{k+1}\big) g \tag{3.24}$$

As will be discussed in section 3.4.4, computation will be particularly easy if we choose W_{k+1} to be a scaled copy of Λ_k with a rank-one update, so we choose W_{k+1} to be of the form:

$$W_{k+1} = \theta \Lambda_k + \alpha g g^T \tag{3.25}$$

α and θ are unknown scalars. θ controls how fast the precision as a whole increases. If we would like the variance in directions other than g to shrink by 9/10, for example, we choose $\theta = 1/9$. Since θ is constant, there will be exponentially fast convergence of the proposal covariance in all directions, which allows quick recovery from overly diffuse initial crumb distributions. For this method, θ is not a critical choice. Setting θ close to zero causes excessively slow convergence when σ_c is large relative to the slice without corresponding benefits when it is small, but a broad range of values larger than zero give similar performance. I generally set θ to one. Substituting equation 3.25 into equation 3.24 gives:

$$\sigma_{k+1}^{-2} = g^T \big(\Lambda_k + \theta \Lambda_k + \alpha g g^T\big) g \tag{3.26}$$

Noting that $g^T g = 1$, we solve for α, obtaining:

$$\alpha = \max\{\sigma_{k+1}^{-2} - (1+\theta) g^T \Lambda_k g, 0\} \tag{3.27}$$

α is restricted to be positive to guarantee positive definiteness of the crumb covariance. (By choosing θ simultaneously, we could perhaps encounter this restriction less frequently,

a possibility I have not explored.) Once we know α, we then compute W_{k+1} using equation 3.25.

The resulting crumb distribution is:

$$c_{k+1} \sim N(x_0, W_{k+1}^{-1}) \tag{3.28}$$

After drawing such a crumb, we draw a proposal according to equations 3.8 to 3.10, accepting or rejecting depending on whether $\ell(x_{k+1}) \geq y_{\text{slice}}$, drawing more crumbs and adapting until a proposal is accepted.

3.4.3 Estimating the density at the mode

We now modify the covariance matching method to remove the restriction that the target distribution be unimodal and remove the requirement that we precompute the log density at the mode. Estimating M each time we update x_0 instead of precomputing it allows M to take on values appropriate to local modes. Since the proposal distribution only approximates the slice even in the best of circumstances, it is not essential that the estimate of M be particularly good.

To estimate M, we initialize M to y_{slice} before drawing the first crumb. Then, every time we fit the parabola described by equation 3.11, we update M to be the maximum of the current value of M and the estimated peak of the parabola. As more crumbs are drawn, M becomes a better estimate of the local maximum. We could also use the values of the log density at rejected proposals and at the $\{u_k\}$ to bound M, but if the log density is locally concave, the log densities at the peaks of the parabola will always be larger than these values.

3.4.4 Efficient computation of the crumb covariance

This section describes a method for using Cholesky factors of precision matrices to make implementation of the covariance matching method of section 3.4.2 efficient. If imple-

mented naively, the method of section 3.4.2 would use $O(p^3)$ operations when drawing a proposal with equation 3.8, a cost we would like to avoid. One way is to represent W_k and Λ_k by their upper-triangular Cholesky factors F_k and R_k, where $F_k^T F_k = W_k$ and $R_k^T R_k = \Lambda_k$.

First, we must draw proposals efficiently. If z_1 and z_2 are p-vectors of standard normal variates, we can replace the crumb and proposal draws of equations 3.28 and 3.8 with:

$$c_k = x_0 + F_k^{-1} z_1 \tag{3.29}$$

$$x_k = \bar{c}_k + R_k^{-1} z_2 \tag{3.30}$$

Since Cholesky factors are upper-triangular, evaluation of $F_k^{-1} z_1$ and $R_k^{-1} z_2$ by backward substitution takes $O(p^2)$ operations.

We must also update the Cholesky factors efficiently. We replace the updates of W_k and Λ_k in equations 3.25 and 3.22 with:

$$F_{k+1} = \text{chud}(\sqrt{\theta} R_k, \sqrt{\alpha} g) \tag{3.31}$$

$$R_{k+1} = \text{chud}(\sqrt{1+\theta} R_k, \sqrt{\alpha} g) \tag{3.32}$$

Here, $\text{chud}(R, v)$ is the Cholesky factor of $R^T R + v v^T$. The function name is an abbreviation for "Cholesky update." It can be computed with the LINPACK routine `DCHUD`, which uses Givens rotations to compute the update in $O(p^2)$ operations (Dongarra et al., 1979, ch. 10).

Finally, we would like to compute the proposal mean efficiently. We do this by keeping a running sum of the un-normalized crumb mean (the parenthesized expression in equation 3.10), which we will represent by $\bar{c}_k^*$. Define:

$$\bar{c}_k^* = W_1 c_1 + \cdots + W_k c_k \tag{3.33}$$

$$= \bar{c}_{k-1}^* + W_k c_k \tag{3.34}$$

$$= \bar{c}_{k-1}^* + F_k^T F_k c_k \tag{3.35}$$

Then, using forward and backward substitution, we can compute the normalized crumb mean, $\bar{c}_k$, as:

$$\bar{c}_k = R_k^{-1} R_k^{-T} \bar{c}_k^* \tag{3.36}$$

This way, we can compute $\bar{c}_k$ in $O(p^2)$ operations and do not need to save all the crumbs and crumb covariances.

With these changes, the resulting algorithm is numerically stable even with ill conditioned target distributions. Each crumb and proposal draw takes $O(p^2)$ operations. Figure 3.5 shows pseudocode for a single iteration.

3.5 Shrinking rank proposals

This section presents a second MCMC method in the crumb framework, shrinking rank. It is simpler than covariance matching, but retains its desirable properties. Like covariance matching, shrinking rank draws a sequence of Gaussian crumbs with mean equal to the current state and variance chosen adaptively based on information from rejected proposals. Instead of attempting to match the curvature of the log density along the gradient, however, it sets the crumb variance in that direction to zero, causing subsequent proposals to have a variance of zero in that direction as well. This technique aims to cause proposal variances to be nonzero only in the longest direction of the slice, which is usually the slowest mixing one.

Each iteration begins by drawing a slice level as discussed in section 3.1:

$$y_{\text{slice}} = \ell(x_0) - E \qquad \text{where } E \sim \text{Exponential}(1) \tag{3.37}$$

When the first crumb, c_1, is drawn, there are no previous proposals providing information to adapt on, so it is drawn from a spherical Gaussian distribution with marginal standard deviation σ_c, where σ_c is a tuning parameter. The distribution for the first proposal, x_1, is also a spherical Gaussian with standard deviation σ_c but centered at c_1 instead of x_0.

One step in the covariance matching method

initialize ℓ, $x_0 \in \mathbb{R}^p$, σ_c, and θ.
$M \leftarrow \ell(x_0)$
$y_{\text{slice}} \leftarrow M - \text{draw from Exponential}(1)$
$R \leftarrow \sigma_c^{-1} I$
$F \leftarrow \sigma_c^{-1} I$
$\bar{c}^* \leftarrow 0$
repeat until a proposal is accepted:
    $z \leftarrow \text{draw from } N_p(0, I)$
    $c \leftarrow x_0 + F^{-1} z$
    $\bar{c}^* \leftarrow \bar{c}^* + F^T F c$
    $\bar{c} \leftarrow R^{-1} R^{-T} \bar{c}^*$
    $z \leftarrow \text{draw from } N_p(0, I)$
    $x \leftarrow \bar{c} + R^{-1} z$
    $y \leftarrow \ell(x)$
    if $y \geq y_{\text{slice}}$:
        accept proposal x.
    end (if)
    $G \leftarrow \nabla \ell(x)$
    $g \leftarrow G / \|G\|$
    $\delta \leftarrow \|x - c\|$
    $u \leftarrow x + \delta g$
    $\ell_u \leftarrow \ell(u)$
    $\kappa \leftarrow -2\delta^{-2} \left(\ell_u - y - \delta \|G\|\right)$
    $\ell_{x,u} \leftarrow \frac{1}{2} \frac{\|G\|^2}{\kappa} + y$
    $M \leftarrow \max\{M, \ell_{x,u}\}$
    $\sigma^2 \leftarrow \frac{2}{3} \frac{M - y_{\text{slice}}}{\kappa}$
    $\alpha \leftarrow \max\left\{0, \sigma^{-2} - (1+\theta) g^T R^T R g\right\}$
    $F \leftarrow \text{chud}\left(\sqrt{\theta} R, \sqrt{\alpha} g\right)$
    $R \leftarrow \text{chud}\left(\sqrt{1+\theta} R, \sqrt{\alpha} g\right)$
end (repeat)

Figure 3.5: A single iteration of the adaptive algorithm of section 3.4. The variables are mostly the same as in the text. The k subscript is dropped since there is no need to keep copies of the values from any but the most recent iteration. The variable $\ell_{x,u}$ indicates the peak of the parabolic cut through x and u.

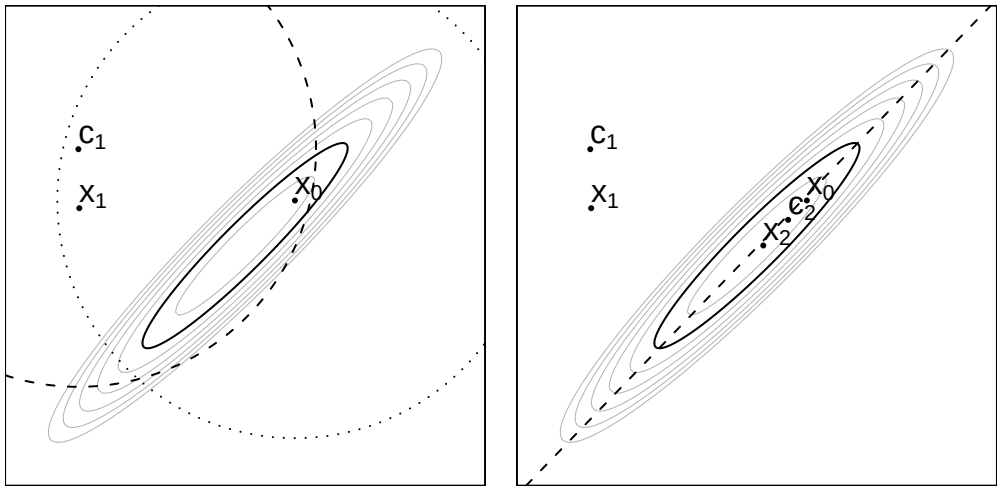

(a) (b)

Figure 3.6: (a) The grey lines represent the contours of a two-dimensional distribution; the solid ellipse represents the boundary of the slice. The first crumb, c_1, is drawn from a spherical Gaussian represented by a dotted circle; a proposal, x_1, is drawn from a spherical Gaussian centered at c_1, represented by a dashed circle. x_1 is rejected because it is outside the solid ellipse. (b) A second crumb, c_2, is drawn from a reduced-rank subspace, represented by a dashed line. A second proposal, x_2, is drawn from the same subspace. Since x_2 is inside the solid ellipse, it is accepted.

If $\ell(x_1)$ is at least y_{slice}, then x_1 is inside the slice and is accepted. Up to this point, the method is identical to covariance matching and Nonadaptive Crumb.

If x_1 is outside the slice, we can use the gradient of the log density at x_1 to determine a distribution for c_2 that leads to a distribution for x_2 that more closely resembles the shape of the slice itself. In particular, we consider setting the variance of the distribution of c_2 to be zero in the direction of the gradient, since the gradients are orthogonal to the contours of the log density. If the contour defined by the log density at the proposal and the contour defined by the slice level are the same shape, this will result in a crumb, and therefore a proposal, being drawn from a distribution oriented along the long directions of the slice. This procedure is illustrated in figure 3.6.

The nullspace of the subspace the next crumb is to be drawn from is represented by J, a matrix with orthogonal, unit-length columns. Let g^* be the projection of the gradient of the log density at a rejected proposal into the nullspace of J. When g^* makes a large angle with the gradient, it does not make sense to adapt based on it, because this subspace is already nearly orthogonal to the gradient. When the angle is small, we extend J by appending $g^*/\|g^*\|$ to it as a new column. Here, we consider an angle to be large if it is greater than 60°, but the exact threshold is not crucial.

Formally, define $P(J, v)$ to be the projection of vector v into the nullspace of the columns of J (so that it returns vectors in the space that crumbs and proposals are drawn from):

$$P(J, v) = \begin{cases} v - JJ^T v & \text{if } J \text{ has at least one column} \\ v & \text{if } J \text{ has no columns} \end{cases} \tag{3.38}$$

We let g^* be the projection of the gradient at the proposal orthogonal to the columns of J:

$$g^* = P\left(J, \nabla \ell(x_k)\right) \tag{3.39}$$

Then we update J if

$$\frac{g^{*T}\nabla\ell(x_k)}{\|g^*\|\,\|\nabla\ell(x_k)\|} > \cos 60^\circ \tag{3.40}$$

and the nullspace of J is not one dimensional. This update to J is:

$$J \leftarrow \begin{bmatrix} J & \frac{g^*}{\|g^*\|} \end{bmatrix} \tag{3.41}$$

To ensure a proposal is accepted in a reasonable number of iterations, if we do not update J for a particular crumb, we scale down σ_c by a parameter, θ, commonly chosen to be 0.95. Write the standard deviation for the kth crumb as $\sigma_{c(k)}$. If we never updated J, then $\sigma_{c(k)}$ would equal $\theta^{k-1}\sigma_c$. Since we only change one of J or the standard deviation each step, $\sigma_{c(k)}$ does not fall this fast. If the standard deviation were updated every step, it would fall too fast in high-dimensional spaces where many updates to J are required before the proposal distribution is reasonable. As a further refinement, we down-scale $\sigma_{c(k)}$ by an additional factor of 0.1 when the density at a proposal is zero. Since the usual form of adaptation is not possible in this case, this scaling results in significantly fewer crumbs and proposals on distributions with bounded support.

After drawing the kth crumb the mean of the distribution for the next proposal is:

$$x_0 + \mu_x = x_0 + P\left(J,\ \frac{\sigma_{c(1)}^{-2}(c_1 - x_0) + \cdots + \sigma_{c(k)}^{-2}(c_k - x_0)}{\sigma_{c(1)}^{-2} + \cdots + \sigma_{c(k)}^{-2}}\right) \tag{3.42}$$

The mean of the proposal distribution is computed as an offset (μ_x) to x_0, but any point in the nullspace of the columns of J would generate the same result. In that space, the offset of the proposal mean is the mean of the offsets of the crumbs weighted by their precisions. The variance of the proposals in that space is the inverse of the sum of the precisions of the crumbs:

$$\sigma_x^2 = \left(\sigma_{c(1)}^{-2} + \cdots + \sigma_{c(k)}^{-2}\right)^{-1} \tag{3.43}$$

Pseudocode for one shrinking rank update is shown in figure 3.7. These updates can be combined with others, as in section 4.3.

One step in the shrinking-rank method

initialize $x_0 \in \mathbb{R}^p$, $\sigma_c \in \mathbb{R}^+$, $\theta \in \mathbb{R}^+$, and $\ell(\cdot) : \mathbb{R}^p \mapsto \mathbb{R}$.
$y_{\text{slice}} \leftarrow \ell(x_0) -$ draw from Exponential(1)
$k \leftarrow 0$
$\sigma_{c(1)} \leftarrow \sigma_c$
$J \leftarrow [\ ]$
repeat until a proposal is accepted:
  $k \leftarrow k + 1$
  $c_k \leftarrow P\big(J, \text{draw from } N_p(x_0, \sigma^2_{c(k)} I)\big)$
  $\sigma_x^2 \leftarrow \left(\sigma_{c(1)}^{-2} + \cdots + \sigma_{c(k)}^{-2}\right)^{-1}$
  $\mu_x \leftarrow \sigma_x^2 \left(\sigma_{c(1)}^{-2}(c_1 - x_0) + \cdots + \sigma_{c(k)}^{-2}(c_k - x_0)\right)$
  $x_k \leftarrow x_0 + P\left(J, \text{draw from } N_p(\mu_x, \sigma_x I)\right)$
  if $\ell(x_k) \geq y_{\text{slice}}$:
    accept proposal x_k.
  end (if)
  $g^* \leftarrow P(J, \nabla\ell(x_k))$
  if $\ell(x_k)$ is not finite:
    $\sigma_{c(k+1)} \leftarrow 0.1 \cdot \theta \cdot \sigma_{c(k)}$
  else if J has fewer than $p - 1$ columns and ${g^*}^T \nabla\ell(x_k) > \cos(60°) \cdot \|g^*\| \, \|\nabla\ell(x_k)\|$:
    $J \leftarrow [\ J \quad g^*/\|g^*\|\ ]$
    $\sigma_{c(k+1)} \leftarrow \sigma_{c(k)}$
  else
    $\sigma_{c(k+1)} \leftarrow \theta \cdot \sigma_{c(k)}$
  end (if)
end (repeat)

Figure 3.7: This pseudocode represents a single transition in the shrinking rank method with log density function $\ell(\cdot)$, starting from state $x_0 \in \mathbb{R}^p$, and with tuning parameters σ_c and θ. The projection function, P, is defined in equation 3.38.

3.6 Evaluation of the proposed methods

Sections 3.2, 3.4, and 3.5 propose new MCMC methods in the hope that they will outperform existing methods. This section uses the graphical technique described in section 2.3 to compare these methods to each other, to Adaptive Metropolis, and to slice sampling with stepping out.

Adaptive Metropolis (Haario et al., 2001) is relevant because the methods of section 3.2 are inspired by it and it performs well on low dimensional targets. Slice sampling with stepping out (Neal, 2003, §4), the other component of the univariate method described in section 3.2.1, is a robust alternative to Metropolis used when Gibbs sampling to update components of distributions whose full conditional is not available.

3.6.1 Comparison on reference distributions

A comparison of these methods on the distributions described in section 2.2.2 is shown in figure 3.8. On the first distribution, GP (unlogged), no sampler performs well. It is unimodal and only three-dimensional, but its components are right-skewed and highly correlated with each other. Estimates of the mean are dominated by extreme values and therefore slow to converge. While some of the methods compared can perform well on highly correlated parameters, they are less efficient when the target distribution has heavy tails.

The next distribution, $N_4(\rho = 0.999)$, is a four-dimensional Gaussian. Its curvature is constant, so methods that make an attempt to understand the local structure up to the first two moments—all except Step-out Slice—perform well when their scale parameters are large enough to take reasonably-sized steps. Shrinking Rank and Covariance Matching are effectively a random walk when their tuning parameters are too small. As a result, as described in section 2.3.2, their cost measures show a slope of -2 until they reach approximately ten, a small factor off the square root of the largest eigenvalue of

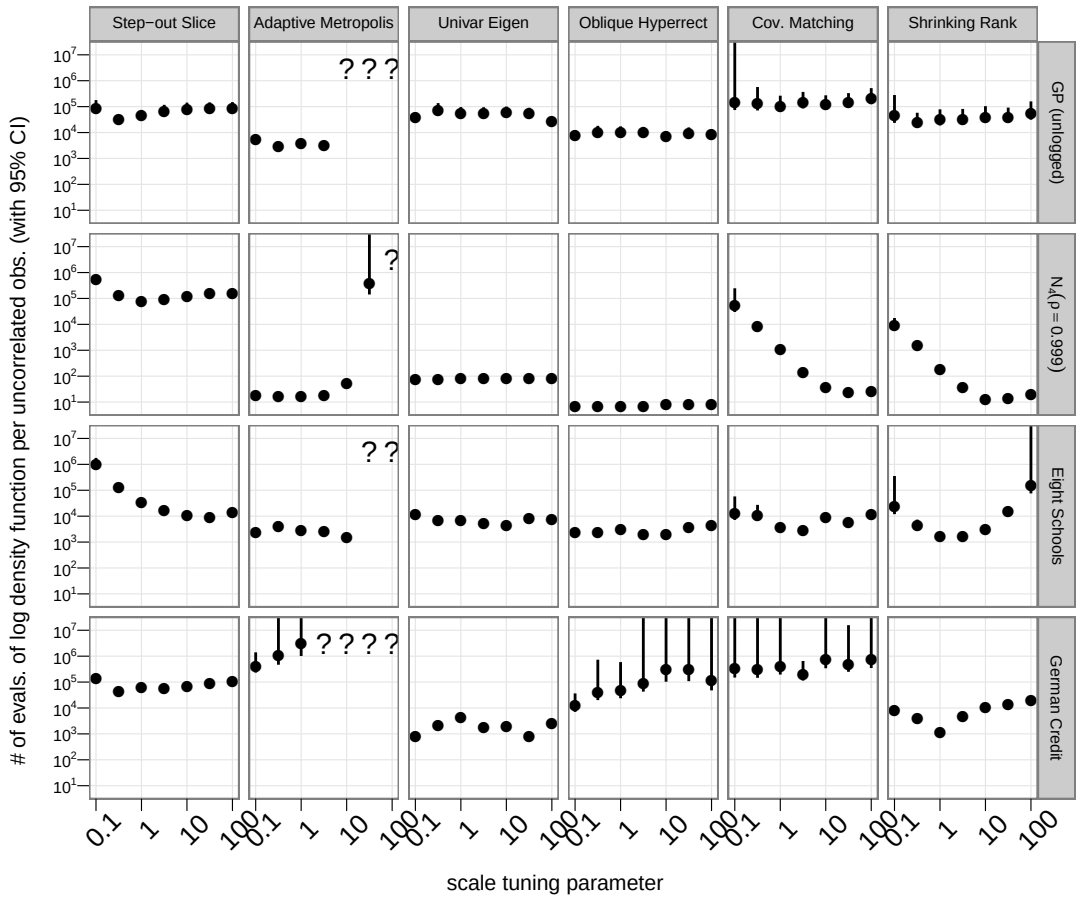

Figure 3.8: A comparison of MCMC methods described in this document to two reference methods using simulations of length 80,000. Section 2.2.2 describes the target distributions. Section 3.6 discusses the results.

the covariance matrix.

The third distribution, Eight Schools, is well conditioned and is not substantially skewed. As a result, every sampler tested performs similarly on it when their tuning parameters are in a reasonable range. As before, the slice samplers that do not do global adaptation (Shrinking Rank, Covariance Matching, and Step-out Slice) perform well for sufficiently large tuning parameters, and Adaptive Metropolis performs well for sufficiently small ones. Globally adaptive slice samplers (Oblique Hyperrect and Univar Eigen) perform well for all tuning parameters tested, assuming they are run long enough to learn the covariance matrix.

The fourth distribution, German Credit, is 25-dimensional, so its covariance has 325 degrees of freedom. Shrinking Rank, Oblique Hyperrect, and Univar Eigen all perform reasonably well on it, but the adaptation required makes their performance more idiosyncratic on German Credit than on other distributions.

3.6.2 Comparison on a latent AR process

This section extends the comparison of section 3.6 by comparing the same six samplers on a family of latent jump-autoregressive processes. In this model, one observes a sequence of N Bernoulli random variables $\{Y_i\}_{i=1}^N$ such that $Y_i = 1$ with probability $1/(1 + \exp(-X_i))$. The $\{X_i\}$ are themselves generated by a mean-zero autoregressive process with an autocorrelation of α, a probability ρ of a jump to an uncorrelated state, and a variance σ^2. The parameters σ^2, α, and ρ are transformed and given Student-t

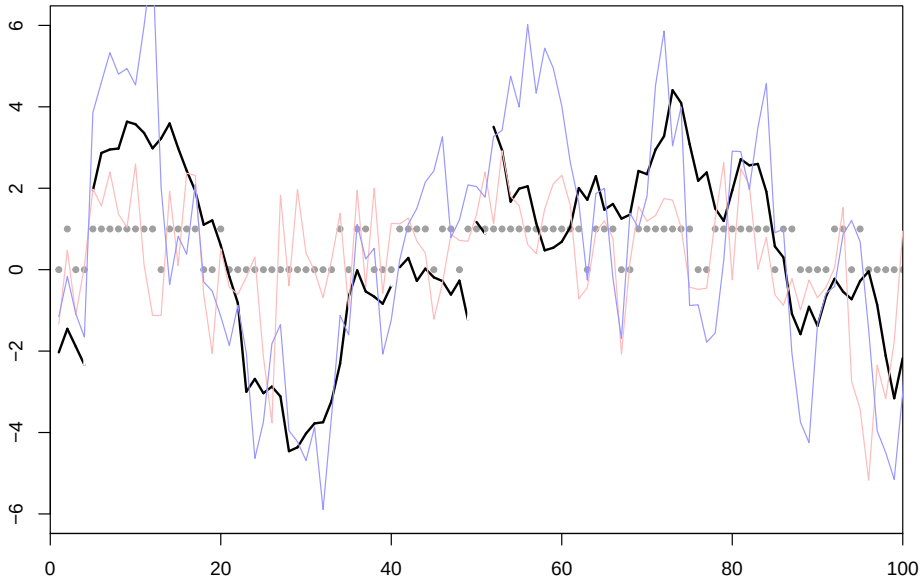

Figure 3.9: A realization of a latent AR process with $\alpha = 0.95$, $\rho = 0.04$, and $\sigma^2 = 2^2$ as described in section 3.6.2. The circles correspond to the $\{Y_i\}$, and the thick line corresponds to the latent $\{X_i\}$ that generated the $\{Y_i\}$. Jumps in the latent process are shown as gaps in the line. In this plot, $N = 100$ and $\rho = 0.04$, so the expected number of jumps is $N \cdot \rho = 4$, which happens to coincide with the actual number. This realization is also used in the $N = 100$ row of figure 3.10. The thin colored lines are draws from the posterior distribution of $\{X_i\}$ given $\{Y_i\}$. Jumps are not explicitly part of the model, so those two lines are not shown with gaps.

priors with four degrees of freedom, loosely following Gelman et al. (2008). Formally:

$$Y_i|X_i \sim \text{Bernoulli}\left(\frac{1}{1+\exp(-X_i)}\right) \quad \text{for } i = 1, \ldots, N \tag{3.44}$$

$$X_i|X_{i-1}, \alpha, \rho, \sigma^2 \sim \begin{cases} N\left(\alpha X_{i-1}, (1-\alpha^2)\sigma^2\right) & \text{with prob. } 1-\rho \\ N\left(0, \sigma^2\right) & \text{with prob. } \rho \text{ or when } i = 1 \end{cases} \tag{3.45}$$

$$\log\left(\frac{\alpha}{1-\alpha}\right) \sim t_4 \tag{3.46}$$

$$\log\left(\frac{\rho}{1-\rho}\right) \sim t_4 \tag{3.47}$$

$$\log \sigma^2 \sim t_4 \tag{3.48}$$

We observe the $\{Y_i\}$ and use an MCMC sampler to simulate $\{X_i\}$, α, ρ, and σ^2. An example of a single realization of such a process is shown in figure 3.9 along with two draws of $\{X_i\}$ given just the same $\{Y_i\}$. This distribution is distinguished from previous distributions in that the correlation between nearby latent variables depends on ρ, α, and σ^2, so global Gaussian approximations are not appropriate. Unlike real-data examples, we can realize $\{Y_i\}$ automatically for a range of N to investigate scaling behavior of samplers.

A comparison of six samplers using latent AR processes of lengths 5, 11, 22, 47, 100, 200, and 400 is shown in figure 3.10. Each process was generated with $\alpha = 0.95$ and $\sigma^2 = 2^2$. The jump probability ρ was chosen so that $N \cdot \rho = 4$, resulting in an expected number of jumps of four for all process lengths. For processes of length 200 and 400, some simulations were not run because they were too slow, particularly those of Adaptive Metropolis.

The most conspicuous pattern is that the tuning parameters tend not to affect the efficiency of sampling much. It is therefore clearer to compare the efficiency of the most efficient simulation in each cell; the results of this comparison are shown in figure 3.11. (The plot is not substantially different if the least efficient simulations are chosen instead.) Shrinking Rank and Cov. Matching outperform the other samplers for longer processes.

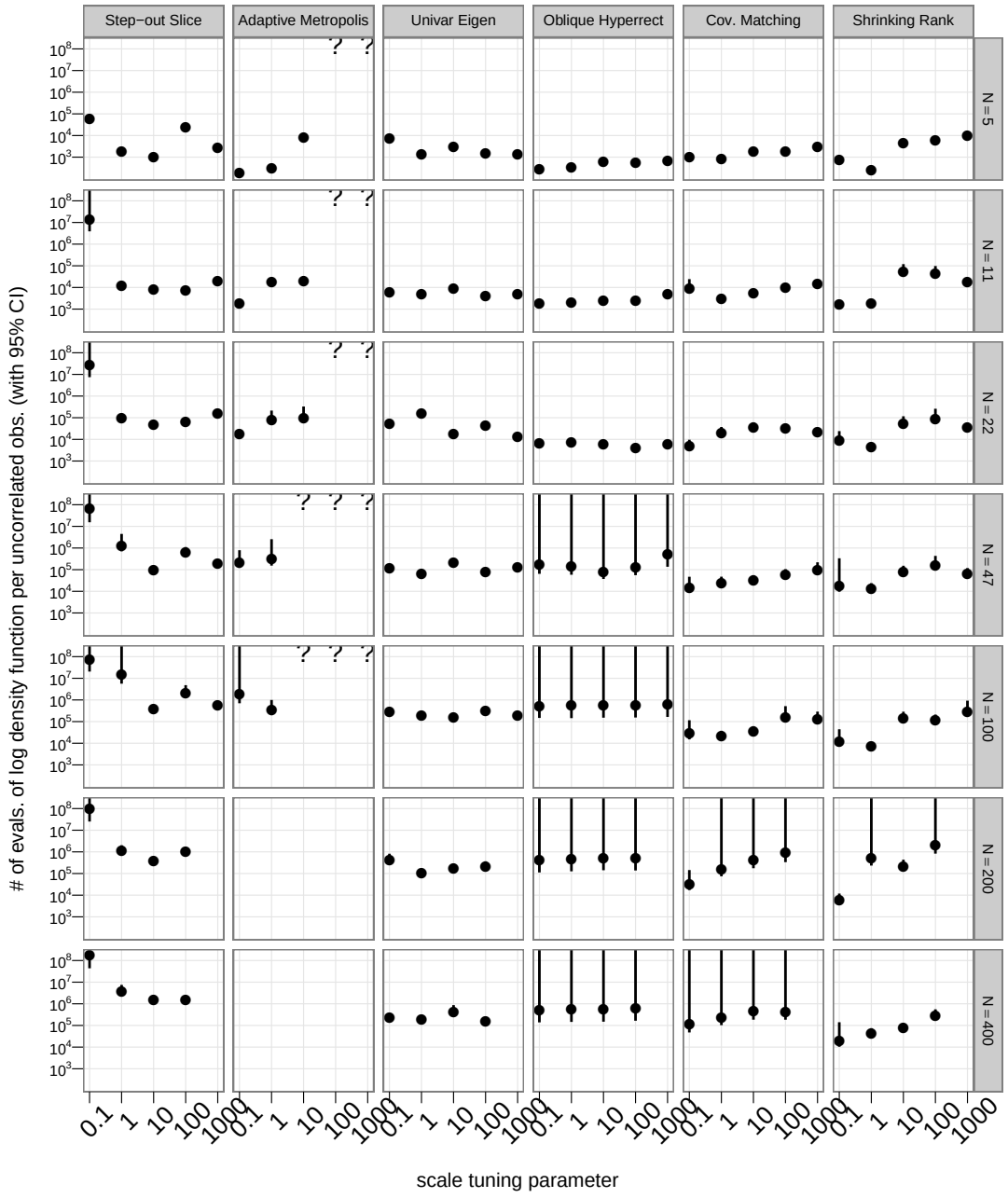

Figure 3.10: A comparison of MCMC methods on the latent AR process described in section 3.6.2. Each row of plots corresponds to a set of simulations with the specified latent process length, N. Including the hyperparameters, the dimension of the target distribution is $N + 3$.

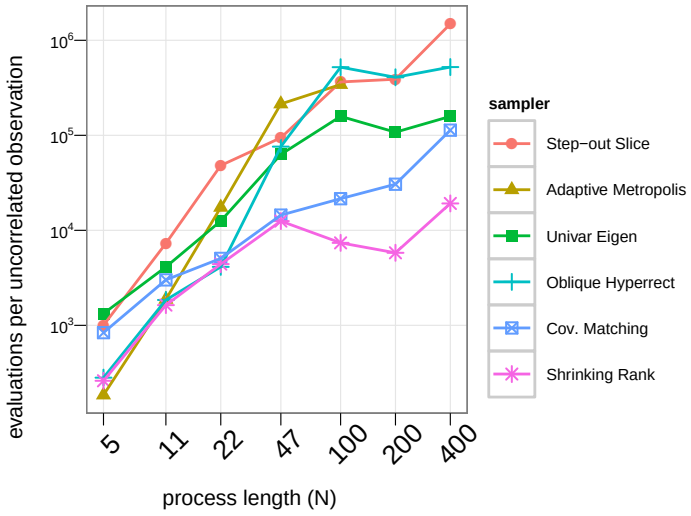

Figure 3.11: A reduced-dimension representation of figure 3.10 showing how performance scales with increasing N. Each plot symbol represents the best-performing simulation for a particular dimension and sampler. See section 3.6.2 for discussion.

Their costs increase more slowly than linearly—about as well as can be hoped for, as discussed in section 4.2. The globally adaptive samplers, Oblique Hyperrect, Univar Eigen, and Adaptive Metropolis, do not fare as well as they do in section 3.6, likely due to the dependence of the correlation structure on the state of the chain.

Chapter 4

Scaling and radial steps

If a random variable X has a log density function $\ell(\cdot)$, then $\ell(X)$ is a scalar random variable. For many p-dimensional probability distributions, this random variable has a standard deviation proportional to $\sqrt{p}$ (Roberts and Rosenthal, 2002; Neal, 2003, pp. 758–760). Multivariate slice sampler updates change the log density by at most $O(1)$ each iteration using the exponential draws of section 3.1, so they take at least $O(p)$ iterations to reach an independent state. (The updates of random-walk Metropolis work differently but scale similarly.) This chapter explores this scaling behavior and proposes methods to improve it. First, it describes the scaling of simple and idealized slice samplers to establish a baseline and to identify proper tuning parameters. Then, it extends the comparison to more realistic distributions and shows how the scaling of practical methods can be improved with radial steps toward or away from a local mode.

4.1 Optimal tuning of Gaussian crumbs

4.1.1 Scaling on slices of known radius

A representative example of a slice sampler that takes multivariate steps is slice sampling with nonadaptive Gaussian crumbs (Neal, 2003, §5.2), on which the covariance matching

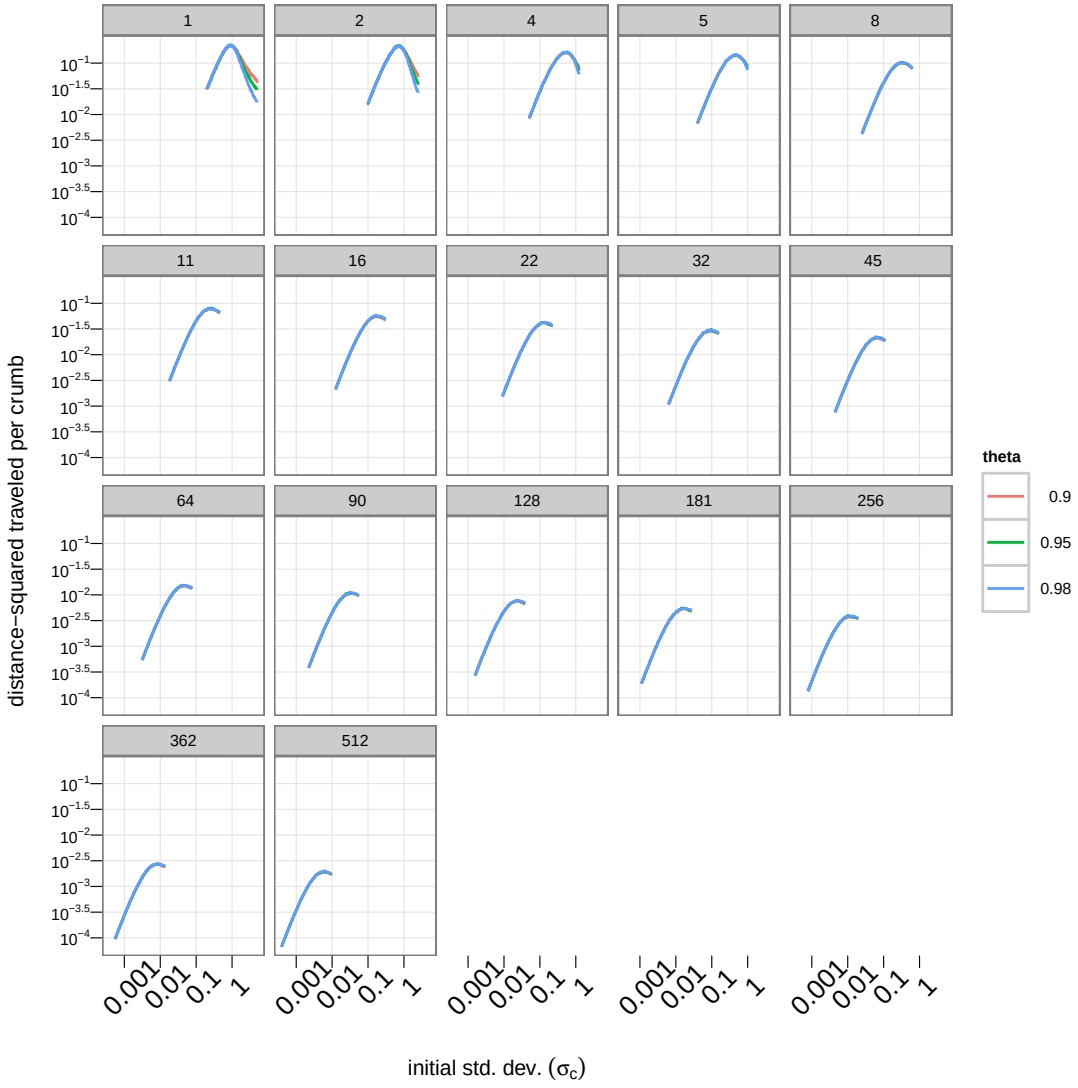

Figure 4.1: Distance squared traveled per crumb-proposal pair on a unit p-ball slice as a function of σ_c and θ, with each cell representing a value of p. Varying θ has little effect, so the lines for each value overlap. See section 4.1.1 for discussion.

method of section 3.4 and the shrinking rank method of section 3.5 are based. The method draws crumbs from a sequence of Gaussians centered at the current state, drawing proposals from the posterior distribution for the current state given the crumbs. While a method in the crumb framework may adapt the crumb distribution based on log densities at rejected proposals (amongst other possibilities) as in sections 3.4 and 3.5, this section focuses on the non-adaptive case where the crumb distribution depends only on how many crumbs have been drawn.

With non-adaptive Gaussian crumbs, there are two free parameters: the standard deviation of the distribution of the first crumb (σ_c) and the rate with which the standard deviation of successive crumbs falls (θ). This section describes an experiment intended to identify reasonable values for these parameters when the shape and scale of the slice is known. Suppose the slice from which we want to draw an update is a p-ball of known radius R, but we do not know its location. Given an initial state x_0, we would like use the Gaussian crumb method to draw a new point from the slice. To do this, for $k = 1, 2, \ldots$, we draw crumb k:

$$c_k \sim N_p\left(x_0, \sigma_{(k)}^2 I\right) \tag{4.1}$$

and then draw proposal k from the posterior distribution of x_0 given the sequence of crumbs, $\{c_1, \ldots, c_k\}$:

$$x_k \sim N_p\left(\bar{c}_k, \Lambda_k^{-1}\right) \tag{4.2}$$

$$\text{where:} \quad \Lambda_k = \left(\sigma_{(1)}^{-2} + \cdots + \sigma_{(k)}^{-2}\right) I \tag{4.3}$$

$$\text{and:} \quad \bar{c}_k = \Lambda_k^{-1}\left(\sigma_{(1)}^{-2} c_1 + \cdots + \sigma_{(k)}^{-2} c_k\right) \tag{4.4}$$

If x_0 is near the edge of the slice, a larger number of proposals will be rejected before one is accepted than if x_0 were in the interior of the slice. So, the optimal crumb standard deviation depends on x_0. Since x_0 is unknown (from the perspective of proposals), we start with a large $\sigma_{(1)}$ and decrease it quickly so that the elements of the proposal variance, Λ_k^{-1}, decrease exponentially rather than linearly in terms of k as would happen if the

crumb standard deviation were constant.

Take the standard deviation of the kth crumb to be of the form:

$$\sigma_{(k)} = \sigma_c \theta^{k-1} R \tag{4.5}$$

Both σ_c and θ can depend arbitrarily on p. For this experiment, I fix the slice radius, R, to one. The method is scale invariant, so by making the standard deviation proportional to the slice radius, the results generalize to any slice known to be a p-ball.

When p is larger than two or three, each individual step is small relative to the scale of the distribution because most of the mass of a p-ball is very close to its surface. As a result, the sequence of states is approximately a random walk. In r steps, a random walk travels $O(\sqrt{r})$ distance, so the correlation between pairs of states of a random walk is minimized by maximizing the expected squared distance of an individual step (Pasarica and Gelman, 2010, §1.2). To determine the σ_c and θ that lead to the highest average squared distance traveled per log density evaluation (of which there is one per crumb-proposal pair), I simulated 5,000 MCMC iterations for a range of θ, σ_c, and p. The results of this experiment are plotted in figure 4.1.

In this experiment and in one that explored θ ranging from 0.01 to 10, the performance does not appear to depend much on θ, as long as it is less than one. Choosing θ to be exactly one leads to qualitatively worse performance, though 0.99 does not. Therefore, I am comfortable fixing θ to be 0.95 for the experiments in this section.

Next, to find the σ_c with the best squared distance traveled per crumb as a function of p with R fixed at one, I fit the following linear model to the optimal σ_c for each p:

$$\log \sigma_c = \beta_0 + \beta_1 \log p + \varepsilon \tag{4.6}$$

For dimensions greater than two, the fit is quite good. A 95% confidence interval for β_1, the exponent on p, is $(-1.01, -0.94)$ with a regression R-squared of 0.997. To simplify, I round $\hat{\beta}_1$ to -1, yielding the following expression for the optimal σ_c:

$$\sigma_c = \frac{2.6}{p} \tag{4.7}$$

Using equation 4.7, we choose the standard deviation of the kth crumb to be:

$$\sigma_{(k)} = 2.6 \cdot 0.95^{k-1} \cdot \frac{R}{p} \tag{4.8}$$

4.1.2 Scaling on slices of χ_p radius

The previous section established optimal tuning parameters for slice sampling with Gaussian crumbs when we know that the slice is a p-ball with radius R. This may not be practical. But, it is not unreasonable to assume we know, through some sort of adaptation, the shape of the slice. If the slices are ellipsoids known up to a unknown scale factor and an unknown translation, the results of section 4.1.1 apply by affine transform of the crumb distribution. However, while we may be willing to approximate the slice with an ellipsoid, and we can estimate the shape of such an ellipsoid using the sample covariance (or a variant that takes into account local structure), we do not know the scale of the slice. That is, even if we know everything there is to know about the target distribution, since the log density may not be normalized, we cannot, in general, determine the scale factor, R, from just the slice level and shape. This section attempts to find an optimal σ_c given p but not R.

A standard p-dimensional Gaussian has log density:

$$\ell(x) = -\frac{\|x\|^2}{2} + C \tag{4.9}$$

C is an unknown constant (equal to $-\frac{p}{2}\log 2\pi$ if the distribution is normalized). Since $\|x\|^2$ has a χ^2_p distribution, slices from this distribution are of the form $\|x\|^2 < R^2$ for some value of R, with the squared slice radii, R^2, having a χ^2_p distribution. So, to find an optimal σ_c and θ, we can simulate R^2 from a χ^2_p distribution instead of setting R to one to see which σ_c and θ lead to the best general performance.

Using this method of generating R, I repeated the experiment of section 4.1.1. The results are shown in figure 4.2. I repeated the analysis of section 4.1.1 to obtain a curve for the the optimal standard deviation for the kth crumb. The resulting fit is

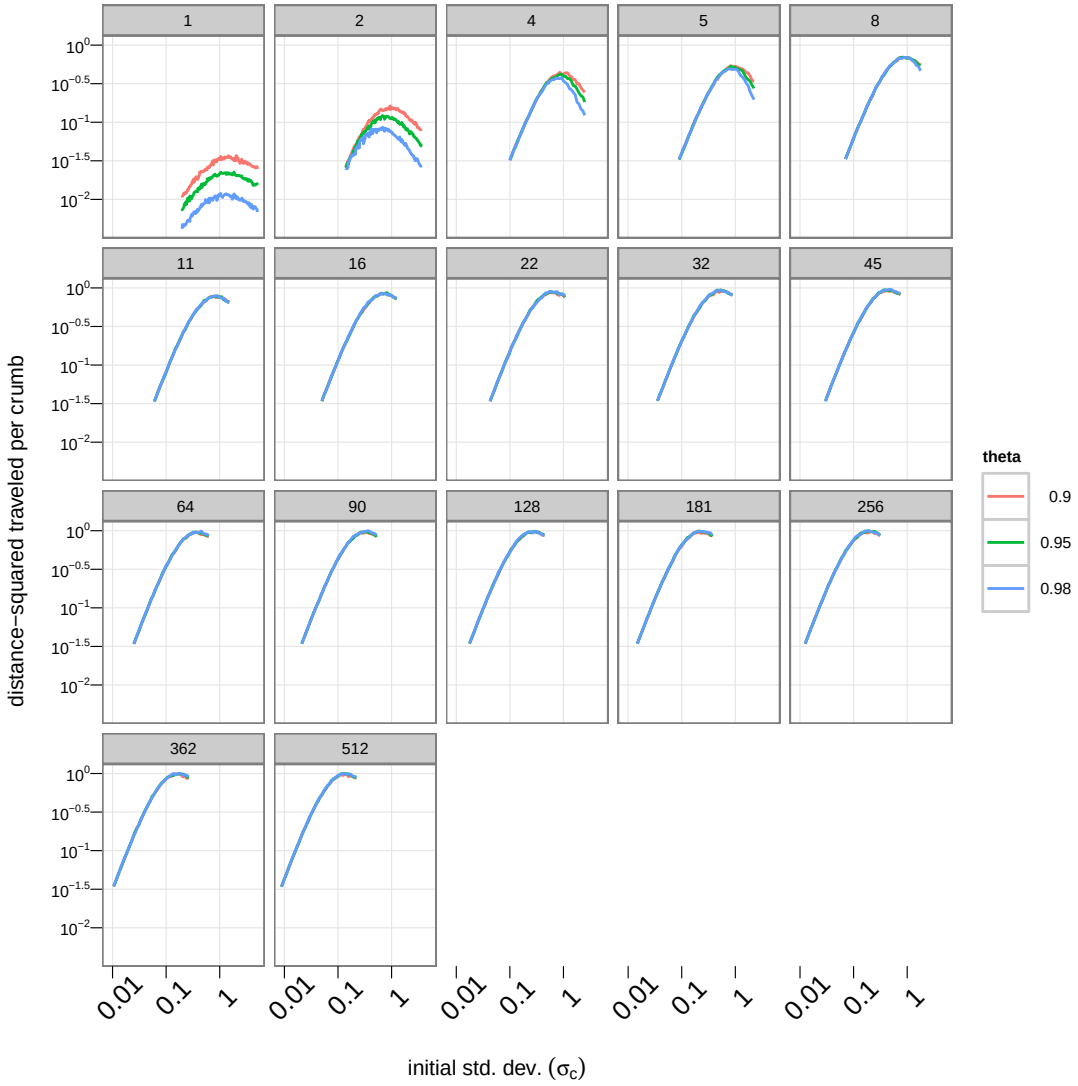

Figure 4.2: Distance squared traveled per crumb-proposal pair on a p-ball slice with radius-squared distributed as χ^2_p as a function of σ_c and θ, with each cell representing a value of p. Varying θ has little effect for the plotted range of σ_c, so the lines for the different θ overlap. See section 4.1.2 for discussion.

also quite good: a 95% confidence interval for the optimal exponent is $(-0.52, -0.42)$ with a regression R-squared of 0.97. Because the optimal proposal standard deviation for random-walk Metropolis with Gaussian proposals is proportional to $p^{-1/2}$ (Roberts et al., 1997), I suspected the same might hold for the optimal initial slice approximation size, so I am comfortable rounding $\hat{\beta}_1$ to $-1/2$, giving the following model, where σ_ℓ is the assumed-spherically-symmetric standard deviation of the target distribution:

$$\sigma_{(k)} = 2.7 \cdot 0.95^{k-1} \cdot \frac{\sigma_\ell}{\sqrt{p}} \tag{4.10}$$

Unlike equation 4.8, equation 4.10 does not depend on R, so it can be used without knowing the normalization of the distribution. The expectation of a χ^2_p random variable is p, so equation 4.10 is nearly the same as what one obtains by taking the expectation of equation 4.8 with respect to R. Empirically, the distance-squared traveled per crumb when R^2 is χ^2_p-distributed is approximately p times larger than when R is held at one. That is, samplers that can compute R, and therefore use equation 4.8, have step sizes that scale similarly to samplers that cannot, and therefore use equation 4.10.

4.2 Comparisons of non-adaptive Gaussian crumb methods

4.2.1 Comparison to ideal slice sampling

Now that we have values for the tuning parameters of the crumb method, we can compare the crumb method to ideal slice sampling with the knowledge that any performance difference could not be overcome by improved tuning—that differences we observe are likely to be properties of the MCMC methods themselves. In this section, both crumb sampling and ideal slice sampling have access to the true distribution variance. Ideal slice sampling uses the location and slice scale as well, drawing the next state directly from the uniform distribution over the p-ball slice. Crumb sampling does not use the

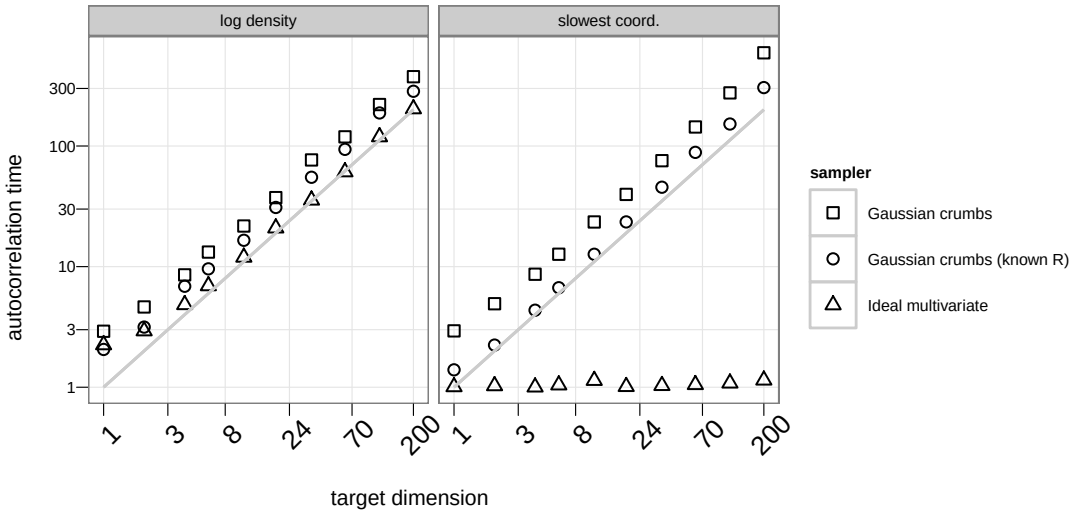

Figure 4.3: Autocorrelation time of simulations of Gaussians plotted against dimension. The left panel shows the autocorrelation time of the log density; the right shows the autocorrelation time of the slowest-mixing coordinate of the distribution. The sloped grey lines represent autocorrelation time being equal to dimension.

location. I include simulations that use the scale (with equation 4.8) and ones that do not (with equation 4.10).

I simulated standard p-dimensional Gaussians for 20,000 iterations for dimensions ranging from 1 to 200. The autocorrelation times of the slowest-mixing component and log density are shown in figure 4.3. The autocorrelation time of individual components is one for the ideal sampler because the states for each individual iteration are uncorrelated. The autocorrelation time is linear in the dimension for the crumb sampler because the states of subsequent iterations are approximately a random walk with step size proportional to $1/\sqrt{p}$. However, the autocorrelation time of the log density scales linearly for both samplers. The crumb sampler is about twice as efficient when it uses the scale of the slice to choose $\sigma_{(k)}$, but both variations scale similarly with dimension. As with other plots in this thesis, figure 4.3 shows the autocorrelation time of the slowest-mixing

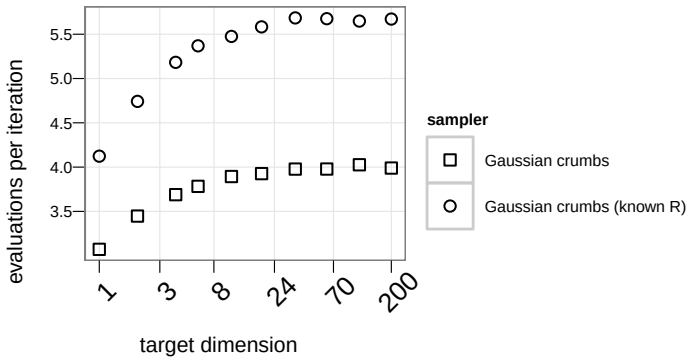

Figure 4.4: The scaling of evaluations per observation for the crumb slice samplers when drawing from Gaussians of increasing dimension when using optimally chosen σ_c and θ.

component. By symmetry, all the components have the same autocorrelation time, so this estimate has a slight positive bias.

To properly compare the performance of the crumb slice sampler in target distributions of different dimensions, one ought to take into account not only the autocorrelation time but also the processor time. As a proxy for processor time, I use log-density function evaluations, as discussed in section 2.2.3. The evaluations per iteration for the crumb sampler are shown in figure 4.4. They do not change significantly with increasing dimension for either variation—the vertical scale is linear, not logarithmic. So, comparing the two crumb variations using only autocorrelation time is reasonable. The number of evaluations per iteration is not well-defined for ideal slice sampling.

One can see in figure 4.4 that the Gaussian crumb method takes more evaluations per iteration on average when it knows R than when it does not because its initial slice approximations tend to be larger. However, this is balanced by the lower autocorrelation times seen in figure 4.3. If one were to compare the product of evaluations per iteration and autocorrelation time, the performances of the two variations would appear even more similar than figures 4.3 and 4.4 imply individually.

4.2.2 Polar slice sampling

Roberts and Rosenthal (2002, §2) discuss the scalability of slice sampling in terms of $Q(y)$, the (p-dimensional) volume of the slice at density y. They show that if $yQ'(y)$ is non-increasing, autocorrelation time is bounded by a constant. They explore this with the distribution with p-dimensional log density $-\|x\|$. For the log density $-\|x\|$, the quantity $yQ'(y)$ is increasing for dimensions larger than one, so it does not have the desirable scaling properties that Roberts and Rosenthal describe. However, neither does the Gaussian distribution. Repeating the experiments described in section 4.2.1, all samplers performed similarly on both this distribution and Gaussian distributions.

One approach to improving the scaling of the autocorrelation time of the log density is the polar slice sampler of Roberts and Rosenthal, which transforms the distribution to one for which $yQ'(y)$ is non-increasing. For example, they transform the density $e^{-\|x\|}$ to $\|x\|^{p-1}e^{-\|x\|}$. However, their method is not directly applicable to most problems. A related alternative is to alternate steps with a standard, untransformed method, such as the ones described in chapter 3, with polar-slice-sampler steps along the line through the current state and the mode. These radial steps are one dimensional, so they can be taken with univariate slice sampling with stepping-out instead of the expensive rejection sampling Roberts and Rosenthal propose. Radial steps are invariant under the target distribution, so if the standard method is ergodic with respect to the target distribution, the combined method will be ergodic as well and will have a less correlated log-density sequence than the standard method.

Pseudocode for a single combined step is shown in figure 4.5. First, a multivariate slice sampler step is taken from x_n to an intermediate state, x_{n+1}^{std}, with a method like the crumb method of section 4.1. Then, a univariate slice sampler step is taken from x_{n+1}^{std} to the next state, x_{n+1}, with a method like stepping out (Neal, 2003, §4) along the line connecting x_{n+1}^{std} and M, the mode of the distribution. Each such step is taken along a line passing through M, so if $\ell(\cdot)$ were used unmodified, points close to M would be

Pseudocode for a combined standard-radial step

$E_1 \leftarrow$ draw from Exponential(1)

$y_{n+1}^{\text{std}} \leftarrow \ell(x_n) - E_1$

$x_{n+1}^{\text{std}} \leftarrow$ uniform invariant update of x_n on $\{x \,|\, \ell(x) \geq y_{n+1}^{\text{std}}\}$

$E_2 \leftarrow$ draw from Exponential(1)

$y_{n+1}^{\text{rad}} \leftarrow (p-1)\log|x_{n+1}^{\text{std}} - M| + \ell(x_{n+1}^{\text{std}}) - E_2$

$x_{n+1} \leftarrow$ uniform invariant update of x_{n+1}^{std} on

$\{x' \,|\, x' = x + \beta(x - M),\ \beta \in \mathbb{R}, \text{ and } (p-1)\log|x' - M| + \ell(x') \geq y_{n+1}^{\text{rad}}\}$

Figure 4.5: Pseudocode for a combination of a step with a standard MCMC method and a radial step of the polar slice sampler. M is the location of the mode. x_{n+1}^{std} can be drawn with any slice sampler that takes multivariate steps; x_{n+1} can be drawn with any slice sampler that takes univariate steps. See section 4.2.2 for discussion.

overrepresented in the sample. The Jacobian factor of the radial transform is $\|\cdot\|^{p-1}$, so when taking radial steps, its log is added to $\ell(\cdot)$ to obtain a log density for radial steps that holds the target distribution invariant. This transform is discussed further by Roberts and Rosenthal (2002, §4).

To investigate whether such steps improve the efficiency of slice sampling with multivariate steps, I repeated the experiments of section 4.2.1, combining radial steps with both the ideal slice sampler and crumb sampling. For crumb sampling, I again set $\theta = 0.95$ and chose σ_c with equation 4.10. The results are compared in figure 4.6. From the right panel, one can see that the radial steps do not affect the autocorrelation time of the individual components of the distribution. However, from the left panel, one can see that the radial steps do reduce the growth in autocorrelation time from linear to constant when alternated with either ideal slice sampling or the Gaussian crumb method. Radial steps do require several evaluations per iteration, roughly as many as steps with Gaus-

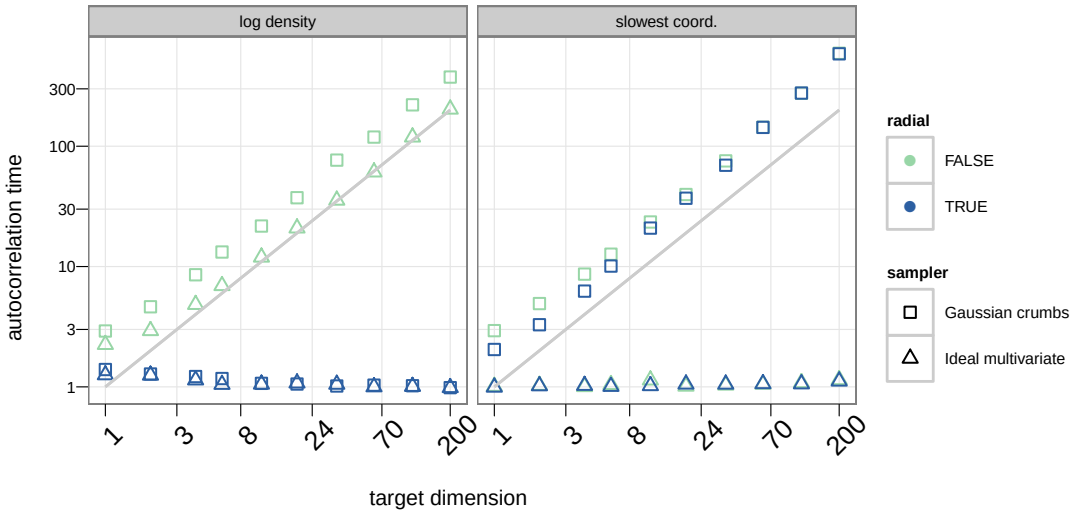

Figure 4.6: Performance of Gaussian crumbs and ideal slice sampling with Gaussian target distributions. (left) Autocorrelation time of log density vs. dimension. (right) Maximum autocorrelation time of components vs. dimension. The sloped grey lines represent autocorrelation time being equal to dimension. See section 4.2.2 for discussion.

sian crumbs. However, the growth of the autocorrelation time with increasing dimension dominates this cost.

4.2.3 Univariate steps

An alternative to the crumb method is slice sampling with univariate updates (Neal, 2003, §4). This section compares the previously described samplers to two variants of slice sampling with univariate updates. The first variant, "Ideal univariate," is an analogue of ideal slice sampling that only moves in one dimension at a time. The second, "Univariate," uses Neal's doubling method to determine the extent of the current slice. The relative advantage of univariate updates depends on whether it is more efficient to evaluate the log density function after changing only one coordinate than it is to evaluate it at an arbitrary point. I will consider both the case where both costs are the same and the case where univariate updates are a factor of p more efficient, as could be the case when full conditional distributions are known. The more efficient variant is denoted by "Efficient univariate."

Figure 4.7 shows the results of this simulation. Assuming the less efficient scenario for univariate updates, the cost measure increases linearly for univariate slice sampling for both components of the target distribution and the log density when slice extents cannot be computed analytically, and nearly linearly when they can be. Radial steps (not plotted) have no effect on this scaling. Univariate steps take a step in the log density direction p times in a sweep through the coordinates rather than once, so a single sweep will travel $O(\sqrt{p})$ in the log density direction instead of $O(1)$, even without radial steps. Unfortunately, so many evaluations are spent updating the individual coordinates that there is no overall efficiency improvement. So, if there is no special efficiency to univariate updates, univariate slice sampling is comparable in performance to crumb sampling without radial steps when we are interested in the efficiency with respect to either the coordinates or the log density. However, if univariate updates are a factor of

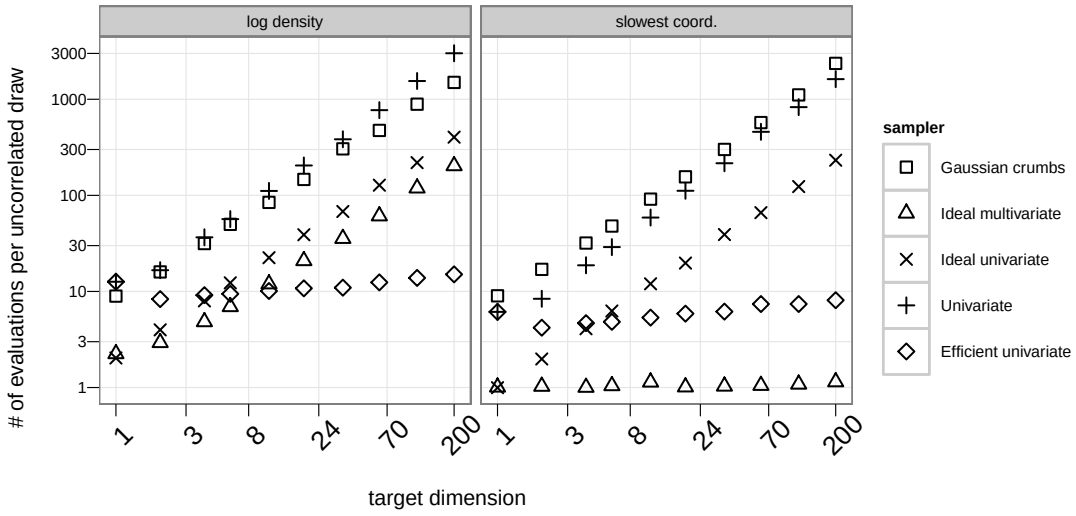

Figure 4.7: Log density evaluations per uncorrelated draw from a Gaussian. The cost measures use the autocorrelation time of the log density and the slowest mixing component of the state space, respectively. The ideal samplers are arbitrarily assumed to evaluate the log density once per iteration. See section 4.2.3 for discussion.

p cheaper than arbitrary updates, they have a clear advantage, scaling similarly to ideal slice sampling with multivariate steps.

4.2.4 Discussion

The Gaussian crumb method is a prototypical slice sampler that uses the shape of a distribution but not the location of its mode. From the experiments of section 4.2.1, it seems that the autocorrelation time of components of a distribution sampled with this method can scale linearly with dimension. One would need to use a method that takes advantage of the location of the mode to allow for methods where the autocorrelation time is roughly constant.

However, even if the location of the mode is known, making a method like the ideal slice sampler plausible, the autocorrelation time of the log density scales linearly with dimension. As seen in section 4.2.2, the scaling of multivariate step methods can be improved to a constant when Gaussian crumbs or ideal slice sampling is combined with the radial steps of the polar slice sampler. The improvements gained changing from crumb to ideal slice sampling and from adding radial steps are independent. Switching from crumb to ideal slice sampling improves the coordinate autocorrelation time scaling from linear to constant, but does not affect the log density autocorrelation time scaling. Combining crumb or ideal sampling with polar slice sampling improves the log density autocorrelation time scaling from linear to constant, but does not affect the coordinate autocorrelation time scaling. If the contours of the target distribution may have substantially different shapes at different log densities or if one is interested in nonlinear functions of state, one must take care to achieve convergence in both the log density and the coordinates.

4.3 Practical algorithms for radial steps

Radial steps as described in section 4.2.2 are not directly useful because they require the distribution to have a single, known mode. This section presents a version of radial steps that relaxes these assumptions.

One could assume there is a single (but unknown) mode and locate it with a multidimensional optimization routine. Then, steps with any sampler can be alternated with radial steps of the type described in section 4.2.2. This approach works well for unimodal distributions. Alternatively, one could run the optimization routine each iteration. Then, the sampler would always take steps toward or away from a local mode. To maintain invariance of the stationary distribution, the sampler would also have to re-run the optimization routine and reject a tentatively-accepted proposal whenever the optimization routine does not find the same mode when starting the search at the proposal. The method to be described in section 4.3.1 is an extension of this idea that allows for caching of the located maxima.

4.3.1 Radial steps using a gridded state space

A multidimensional optimization each iteration will dominate the cost of the sampler. One partial solution is to grid the state space and cache the maximum found starting from each cell. Denote the current state by x_0. To find a mode, start the optimization routine from the center of the grid cell that the current point is in, x_0'; denote the resulting maximum by M_0. The next time a mode is needed for any point in the same grid cell, the maximum is known to be M_0, and no optimization need be done. The challenge with this approach is to identify a grid size, e, small enough for grid cells not to cover multiple modes but large enough for caching to provide a benefit. Unfortunately, even for very large grid sizes, the number of grid cells is exponential in the dimension unless one cell spans the entire state space. So, caching gives the greatest benefit in low dimensional

state spaces, when the radial steps are least necessary.

Pseudocode for a single gridded radial step is shown in figure 4.8. Subscripts of 0 represent aspects of the current state in $\mathbb{R}^p$; subscripts of 1 represent aspects of a proposal. The symbol 1_p represents a p-dimensional vector of ones, so that $e\lfloor x/e \rfloor + (e/2) \cdot 1_p$ computes the center of the grid cell with edge length e containing the p-vector x. The details of maximization are left out; BFGS (Nocedal and Wright, 2006, ch. 6) is a reasonable method. Stepping out from x_0 to find $R_{\min}$ and $R_{\max}$ is similar to the stepping out method described by Neal (2003, §4), but instead of finding a log density less than y_{slice} in each direction from x_0, we search for x such that $(p-1)\log\|M_0 - x\|$ plus the log density is less than y_{slice} since we are using polar slice sampling steps. The logged Jacobian factor, $(p-1)\log\|M_0 - x\|$, is the same as the one described in section 4.2.2. $R_{\min}$ and $R_{\max}$ are taken to be negative and positive offsets from x_0; the endpoints of the slice approximation are at $x_0 + R_{\min} g_0$ and $x_0 + R_{\max} g_0$.

4.3.2 Radial steps using auxiliary variables

This section describes two more variations on radial steps. Like gridded radial steps, they can be alternated with a standard method as demonstrated in figure 4.5. The first such method, "Random Pole," draws a point, c, from a spherically symmetric Gaussian centered at the current state, x_0, with standard deviation σ_c, a tuning parameter. It then takes a radial step along the line connecting x_0 and c, just as the previous method takes a radial step along the line connecting x_0 and M_0. To hold the target distribution invariant, we must make transitions from x_0 to the next state after drawing c equally likely as transitions from the next state to x_0 after drawing c. So, we must multiply the density for drawing c to the target density, or equivalently, add the log density for drawing c to the log density. Because this is a radial step, we must also add the Jacobian

Pseudocode for a gridded radial step

initialize p, e, x_0, and ℓ, where $x_0 \in \mathbb{R}^p$, $e \in \mathbb{R}^+$, and $\ell : \mathbb{R}^p \mapsto \mathbb{R}$.

$x'_0 \leftarrow e \cdot \lfloor x_0/e \rfloor + (e/2) \cdot 1_p$

$M_0 \leftarrow$ local maximum of $\ell(\cdot)$ starting search from x'_0.

$g_0 \leftarrow (M_0 - x_0)/\|M_0 - x_0\|$

$E \leftarrow$ draw from Exponential(1)

$y_{\text{slice}} \leftarrow (p-1) \log \|M_0 - x_0\| + \ell(x_0) - E$

find $R_{\min}$ and $R_{\max}$ by stepping out along g_0.

repeat until a proposal is accepted:

  $R \leftarrow$ draw from Uniform$(R_{\min}, R_{\max})$

  $x_1 \leftarrow x_0 + R \cdot g_0$

  $x'_1 \leftarrow e \cdot \lfloor x_1/e \rfloor + (e/2) \cdot 1_p$

  $M_1 \leftarrow$ local maximum of $\ell(\cdot)$ starting search from x'_1.

  if $M_0 \approx M_1$ and $(p-1) \log \|M_0 - x_1\| + \ell(x_1) > y_{\text{slice}}$:

    accept the proposal, x_1.

  end (if)

  if $R < 0$:

    $R_{\min} \leftarrow R$

  else:

    $R_{\max} \leftarrow R$

  end (if)

end (repeat)

Figure 4.8: Pseudocode for a gridded radial step; see section 4.3.1 for discussion.

term as before. The resulting log density is:

$$\ell^*(x) = (p-1)\log\|c-x\| + \ell(x) - \frac{1}{2}\frac{\|x-c\|^2}{\sigma_c^2} \tag{4.11}$$

The first term is the Jacobian for the radial transform, the second is the underlying log density, and the third is the log density for drawing c from x. First, a slice level is drawn:

$$y_{\text{slice}} = \ell^*(x_0) - E, \quad E \sim \text{Exponential}(1) \tag{4.12}$$

The slice is therefore $\{x \mid \ell^*(x) \geq y_{\text{slice}}\}$. Stepping out (Neal, 2003, §4) is used to find the endpoints of the slice approximation on the line $\{x_0 + \beta(c - x_0) \mid \beta \in \mathbb{R}\}$. Finally, a univariate slice transition is performed between the endpoints, as described by Neal. This is similar to the gridded method of section 4.3.1, except the method for finding the line to search on is different, and the gridded method does not need a density adjustment to account for the differing probabilities of drawing c, since every proposal that is considered by that method uses the same local maximum.

A second auxiliary variable method, "1D Pole," attempts to substitute a one dimensional maximization for the p-dimensional maximization of section 4.3.1. It draws c as with Random Pole and computes the gradient at c, $g = \nabla\ell(c)$. A parabola through c and $c + \alpha g$, for any nonzero α, has three degrees of freedom. By fixing the log densities at c and $c+\alpha g$ and the slope at c, which is $\|g\|$, we can find M_c, the maximum along the approximately parabolic cut through $\ell(\cdot)$. Then, as with Random Pole, 1D Pole takes a radial step along the line connecting x_0 and M_c. It uses the log density:

$$\ell^{**}(x) = (p-1)\log\|M_c - x\| + \ell(x) - \frac{1}{2}\frac{\|x-c\|^2}{\sigma_c^2} \tag{4.13}$$

Since the transition is along a line connecting x_0 and M_c, the Jacobian adjustment (the first term) must use M_c, but since M_c is determined from c, the adjustment for the auxiliary variable (the third term) must use c. I choose α to be one somewhat arbitrarily; the method is not sensitive to its choice on distributions with roughly concentric contours. In addition, $\|M_c - x_0\|$ is restricted to be less than $100 \cdot \sigma_c$, ensuring that floating-point roundoff does not cause all proposals to be rejected when the gradient is very steep.

4.3.3 Evaluation on a sequence of Gaussians

This section shows how the methods of section 4.3.1 and 4.3.2 can be combined with the covariance matching slice sampler of section 3.4 to create a sampler that mixes efficiently with respect to both the state space and log density. Figure 4.9 compares four samplers, one implementing the standard covariance matching method and three where covariance matching steps were alternated with steps described in section 4.3.1 and section 4.3.2. Two variations on gridded radial steps are included: one that uses conjugate gradient (Fletcher and Reeves, 1964) and one that uses BFGS (Nocedal and Wright, 2006, ch. 6). The target distributions are a sequence of Gaussians, each with marginal variances from one to one hundred with uniformly spaced logarithms. For example, the three-dimensional distribution has marginal variances 1, 10, and 100. The components of the test distributions are uncorrelated, but since the methods tested are rotationally invariant except for the minor effect of grid cell alignment when using gridded radial steps, this does not affect the results. The alignment of the grid and the mode of the target distributions is such that even with large grid sizes, the number of grid cells visited is still exponential in the target dimension.

The scale tuning parameter determines σ_c for covariance matching, σ_c for 1D Pole and Random Pole, and e for Grid Cov. Match. The methods' performance on a given measure was not sensitive to their tuning parameters, but occasionally different tuning parameters worked better for different cost measures, so I include two sets of plots. In general, one need only ensure that σ_c be at least the same order of magnitude as the largest marginal standard deviation. Further experiments with tuning parameters chosen independently had results that were substantially the same as those plotted in figure 4.9.

Whether one optimizes for fast mixing of the log density or the slowest mixing coordinate, the samplers perform similarly with respect to the slowest-mixing coordinates, with costs scaling approximately quadratically with dimension. This is dominated by increasing autocorrelation time, which grows approximately as $p^{3/2}$. As discussed in sec-

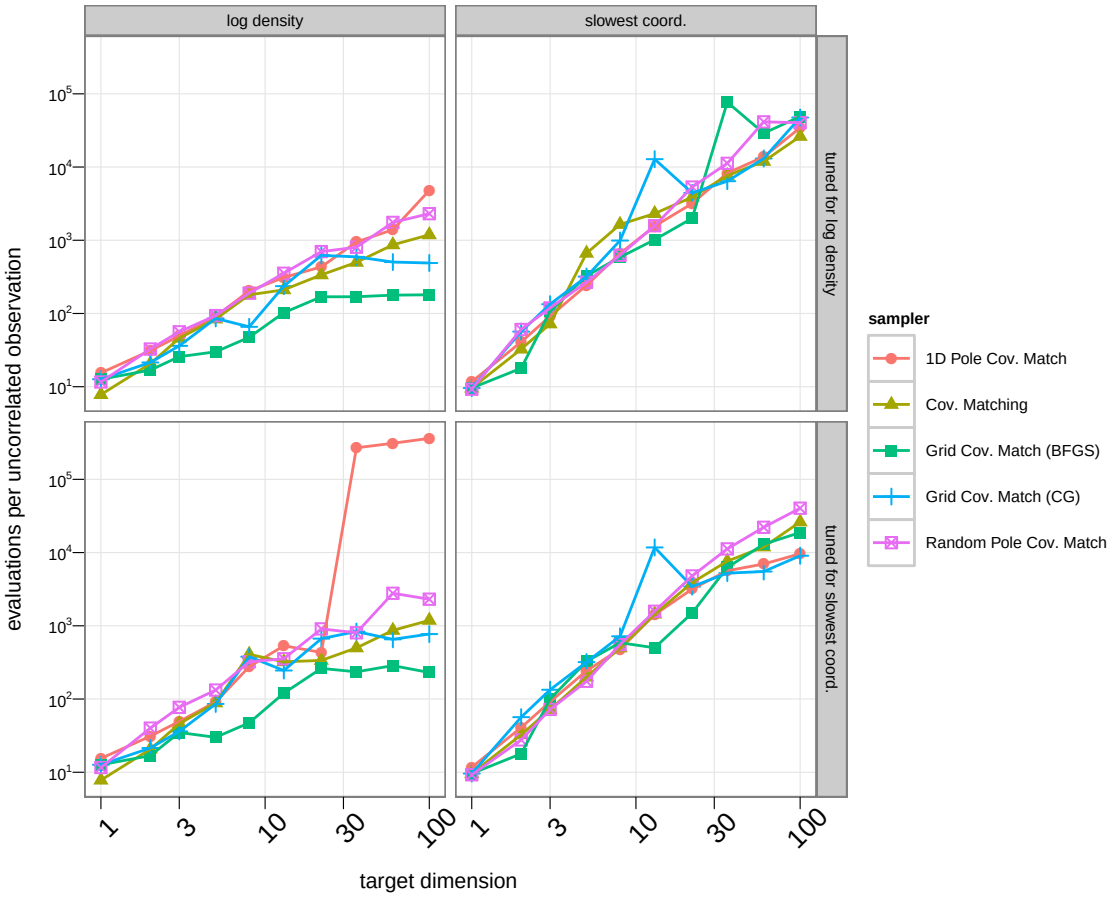

Figure 4.9: Evaluations per uncorrelated observation of variations on covariance matching as a function of target dimension. The plots display the cost for the log density (left) and the slowest-mixing coordinate (right). They compare the base covariance matching method to covariance matching with the three variations on radial steps described in sections 4.3.1 and 4.3.2. Each method was run with a variety of tuning parameters; the best-performing simulation for each was chosen based on either the autocorrelation time of the log density (top) or the slowest-mixing coordinate (bottom). See section 4.3.3 for discussion.

tion 4.2.2, this would not be better than linear in p even if the target distributions were spherically-symmetric Gaussians. Evaluations per iteration grow approximately as $p^{1/2}$; the relation is somewhat flatter in higher dimensions as the cost of a single optimization levels out and the elements of the crumb covariance used by covariance matching steps become dominated by θ-induced shrinkage rather than the parabolic approximations to the log density.

The cost to obtain an uncorrelated log density is roughly linear in the dimension for all methods except covariance matching with gridded radial steps, for which it is constant. The autocorrelation time for the log density in simulations that use either variant of gridded radial steps is effectively one for all dimensions; the increase in cost before the curve flattens reflects the extra evaluations spent on optimization. It seems that radial steps must be taken towards a mode for them to have the desired affect. Similar experiments interleaving gridded radial steps with steps from the oblique hyperrectangle method, described in section 3.2.3, and the shrinking rank method, described in section 3.5, suggest the scaling seen in figure 4.9 is more broadly generalizable.

In high dimensional target spaces, the mixing of coordinates in the target state space tends to be slower than the mixing of the log density, especially when gridded radial steps are used. One might prefer to take several steps in the target state space between single radial steps to minimize the added cost of the radial steps while retaining their benefit.

In the experiment plotted in figure 4.9, the marginal variances are geometrically spaced. In a supplementary experiment, I simulated several other patterns. Grid Cov. Match performs well for any pattern. 1D Pole Cov. Match performs comparably well only when there is at most one marginal variance larger than the smallest ones, such that a one-dimensional search will be able to nearly attain the maximum log density from any initial state.

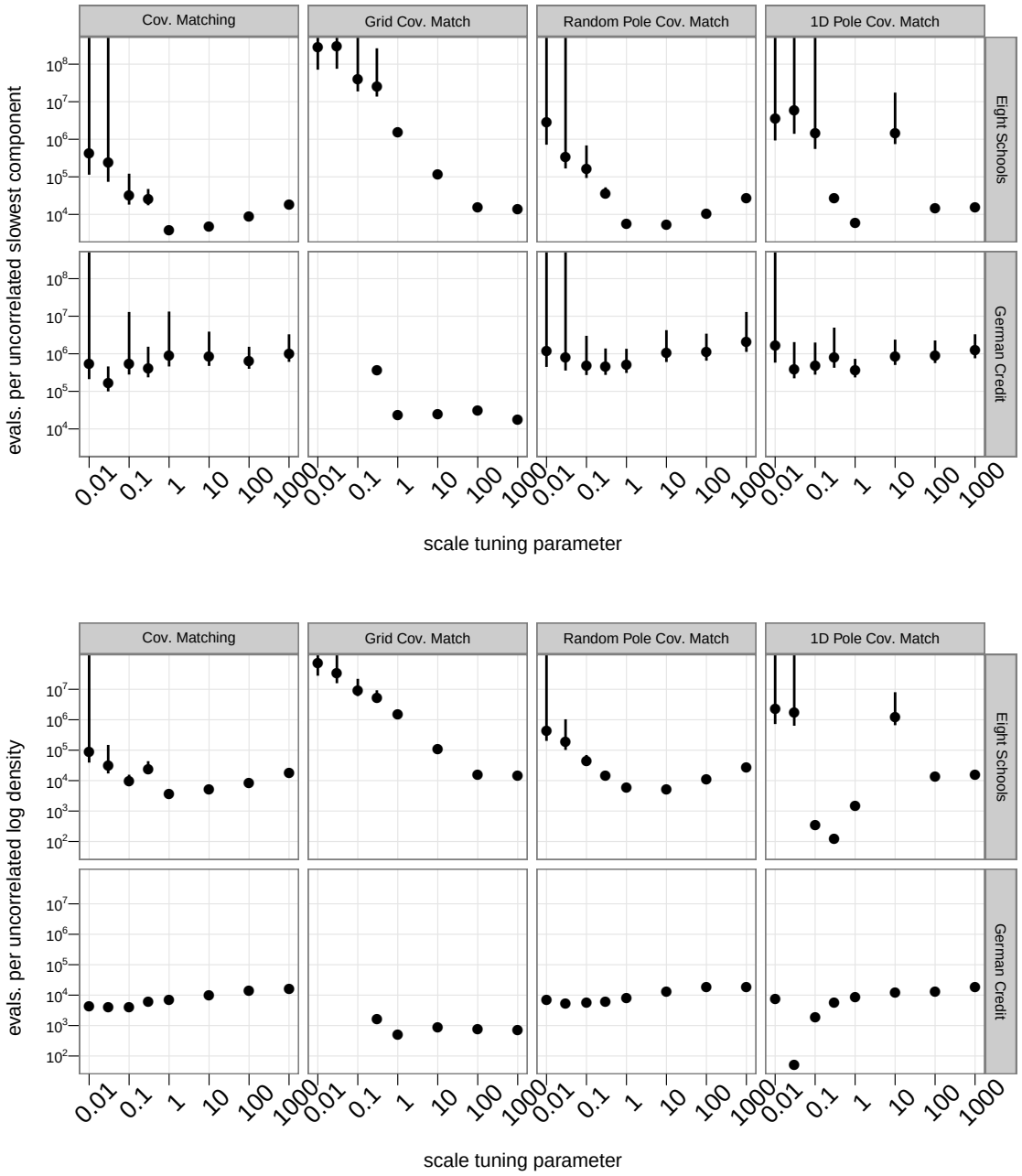

Figure 4.10: Costs of running covariance matching with three radial step methods when simulating from two regression parameter distributions. The top panel shows mixing efficiency in the state space; the bottom panel shows mixing efficiency of the log density. See section 4.3.4 for discussion.

4.3.4 Evaluation on two regressions

To see whether alternating with radial steps is useful on more realistic distributions, not just Gaussians, I ran a set of simulations on the Eight Schools and German Credit examples introduced in section 2.2.2. Figure 4.10 shows the results. As in section 4.3.3, the scale tuning parameter determines the crumb standard deviations, initial slice approximation sizes for radial steps, and the grid edge sizes for gridded radial steps, though the results do not change if they are varied independently. In this experiment, only the BFGS variant of Grid Cov. Match is included. As with the previous experiment, Random Pole Cov. Match performs similarly to standard covariance matching. 1D Pole Cov. Match performs similarly except when precisely tuned. The initial point chosen for the search, c, must be close enough to the current state, x_0, for the gradients at c and x_0 to be similar but far enough away that radial steps can cover a non-negligible distance. Grid Cov. Match does not depend on its tuning parameter to take large steps; varying its tuning parameter affects the evaluations per iteration much more than the autocorrelation time. Grid Cov. Match is generally more efficient with respect to the log density on German Credit. Since German Credit is a higher-dimensional distribution, and radial steps are intended to improve scaling with dimension, this is consistent with earlier results.

Chapter 5

Conclusion

5.1 Contributions

This thesis presents three principal results. First, in chapter 2, I demonstrate a method for comparing MCMC samplers in more depth and clarity than the dominant methods in the literature. By using multi-panel graphics rather than tables of numbers, my method allows researchers to see how new methods compare to established ones in a variety of conditions, limited by processor time more than other considerations.

Second, in chapter 3, I demonstrate several new variations on slice sampling, all of which take multivariate steps using only the log density of a target distribution or the log density and its gradient. Methods based on the eigendecomposition of the sample covariance matrix perform similarly to Adaptive Metropolis, sampling efficiently on distributions with highly correlated components and moderate skewness. Like Adaptive Metropolis, they are globally adaptive, so they may not be appropriate for updating a subset of the components of the state space. And, like Adaptive Metropolis, they cannot be used when the target density is of a dimension where operations on the sample covariance are impractical. Since slice samplers can expand and contract slice approximations in a more straightforward way than Metropolis samplers can expand and contract proposal

densities, they are less dependent on tuning. As a result, the eigendecomposition-based methods are a promising alternative to Adaptive Metropolis.

Later in chapter 3, I demonstrate how the crumb framework can be used to construct samplers that can be embedded in a larger sampling scheme and perform well when the local curvature of the target distribution is not well-captured by a global covariance. These methods, covariance matching and shrinking rank, perform similarly to the eigendecomposition-based methods but without global adaptation, though they do require the gradient of the log density, not just the log density. However, they can be embedded in a larger sampling scheme and are shown to perform well on target distributions where the correlation structure varies throughout the state space. As a result, they are applicable to an even wider variety of densities than the eigendecomposition-based methods. In addition, the shrinking rank method does not store a covariance matrix at any point, so it is suitable for higher-dimensional distributions than eigendecomposition methods and covariance matching. This method has displaced all others for my own use when sampling from distributions with computable gradients.

One way to compute the gradient of a log density function is automatic differentiation; see Nocedal and Wright (2006, §8.2) for an introduction or Griewank and Walther (2008) for a more comprehensive treatment. Unfortunately, it is not a mature field. The `deriv` R function can compute derivatives of simple expressions, but it is not general enough for most log densities. At this point, users must still implement gradient functions by hand. While tedious to write, they can be easily checked for correctness with discrete approximation.

Finally, in chapter 4, I consider the effect of increasing dimension on the performance of slice sampling with multivariate steps and demonstrate a practical way to apply the polar slice sampler, which until now was not practical to implement. I argue that the number of log density evaluations required to obtain an uncorrelated observation scales linearly with dimension in most samplers, whether one considers correlation with respect

to the components of the distribution or the log density. The scaling behavior of the log density can be improved by alternating MCMC steps from a gradient-based sampler like shrinking rank, covariance matching, or reflective slice sampling (Neal, 2003, §7) with the radial steps of the polar slice sampler. For the common case where the target distribution does not have a single, known mode, this section shows how steps can use multidimensional optimization to take radial steps in a way that leaves the target distribution invariant. If one knows the true shape of the slice, a more difficult condition than knowing the location of a local mode, scaling with respect to the coordinates can be improved similarly. These are independent effects; improving one aspect of scaling does not tend to affect the other.

Together, these results are one step towards the goal of generally applicable Markov chain Monte Carlo. I hope that other researchers find the methods of model comparison useful in their own analyses and the sampling methods useful on their own distributions, ultimately improving the ability of non-specialist end users to analyze data with a broader range of models than is currently technically feasible.

5.2 Limitations and future work

While the methods described in this thesis are designed to be fairly general, they assume that the target distribution is continuous. They do not depend on unimodality for correctness, but they do not make any attempt to move efficiently between modes. They can, however, be used as part of a larger sampling scheme that uses, for example, Gibbs sampling to update discrete components and simulated tempering (Marinari and Parisi, 1992) to move between modes.

For some distributions, alternating traditional MCMC steps with gridded radial steps can improve scaling with respect to the log density. However, efficiency is improved only if lines through the current state and a local maximum cut across density contours. This

requires that local maxima be identifiable with relatively few function evaluations. In an attempt to make such steps more efficient and reflective of local structure, I am presently working on an MCMC method that takes moves along a perturbed gradient, analogously to the steepest ascent method for multidimensional maximization. I hope to extend this method to one where sequential steps are orthogonal, analogous to quasi-Newton methods like BFGS (Nocedal and Wright, 2006, ch. 6).

5.3 Software

- ACTCompare is an R package that compares methods for computing autocorrelation time, as in section 2.1. It is available at the author's website, http://www.utstat.toronto.edu/mthompson.

- SamplerCompare is an R package for comparing MCMC samplers, as described in section 2.3. It includes R implementations of the covariance matching method, univariate sampling along eigenvectors, and the oblique hyperrectangle method and a C implementation of the shrinking rank method. It is available from CRAN at http://cran.r-project.org/web/packages/SamplerCompare/index.html.

- A demonstration implementation of covariance matching with gridded radial steps is available at http://www.utstat.toronto.edu/mthompson/gridded-radial.R.

References

Boyd, S. and Vandenberghe, L. (2004). *Convex Optimization*. Cambridge University Press.

Dongarra, J. J., Moler, C. B., Bunch, J. R., and Stewart, G. W. (1979). *LINPACK User's Guide*. Society for Industrial and Applied Mathematics.

Feller, W. (1968). *An Introduction to Probability Theory and its Applications, Volume I, Third Edition*. John Wiley and Sons.

Fishman, G. S. (1978). *Principles of Discrete Event Simulation*. John Wiley and Sons.

Fletcher, R. and Reeves, C. M. (1964). Function minimization by conjugate gradients. *Computer Journal*, 7:148–154.

Gelman, A., Carlin, J. B., Stern, H. S., and Rubin, D. B. (2004). *Bayesian Data Analysis, Second Edition*. Chapman and Hall/CRC.

Gelman, A., Jakulin, A., Pittau, M. G., and Su, Y.-S. (2008). A weakly informative default prior distribution for logistic and other regression models. *The Annals of Applied Statistics*, 2(4):1360–1383.

Gelman, A. and Rubin, D. B. (1992). Inference from iterative simulation using multiple sequences. *Statistical Science*, 7(4):457–511.

Geyer, C. J. (1992). Practical Markov chain Monte Carlo. *Statistical Science*, 7(4):473–511.

Gilks, W. R., Best, N. G., and Tan, K. K. C. (1995). Adaptive rejection Metropolis sampling within Gibbs sampling. *Applied Statistics*, 44(4):455–472.

Gilks, W. R. and Wild, P. (1992). Adaptive rejection sampling for Gibbs sampling. *Journal of the Royal Statistical Society. Series C (Applied Statistics)*, 41(2):337–348.

Girolami, M. and Calderhead, B. (2011). Riemann manifold Langevin and Hamiltonian Monte Carlo. *Journal of the Royal Statistical Society B*, 73:1–37. arXiv:0907.1100v1 [stat.CO].

Golub, G. H. and Van Loan, C. F. (1996). *Matrix Computations, Third Edition*. Johns Hopkins University Press.

Griewank, A. and Walther, A. (2008). *Evaluating Derivatives: Principles and Techniques of Algorithmic Differentiation, Second Edition*. SIAM.

Grötschel, M., Lovász, L., and Schrijver, A. (1993). *Geometric Algorithms and Combinatorial Optimization, Second Corrected Edition*. Springer–Verlag.

Haario, H., Saksman, E., and Tamminen, J. (2001). An adaptive Metropolis algorithm. *Bernoulli*, 7(2):223–242.

Heidelberger, P. and Welch, P. D. (1981). A spectral method for confidence interval generation and run length control in simulations. *Communications of the ACM*, 24(4):233–245.

Mallows, C. L. (1973). Some comments on Cp. *Technometrics*, 15(4):661–675.

Marinari, E. and Parisi, G. (1992). Simulated tempering: A new Monte Carlo scheme. *Europhysics Letters*, 19(6):451–458.

Neal, R. M. (1993). Probabilistic inference using Markov chain Monte Carlo methods. Technical Report CRG-TR-93-1, Dept. of Computer Science, University of Toronto.

Neal, R. M. (2003). Slice sampling. *The Annals of Statistics*, 31:705–767.

Nocedal, J. and Wright, S. J. (2006). *Numerical Optimization, Second Edition*. Springer.

Pasarica, C. and Gelman, A. (2010). Adaptively scaling the Metropolis algorithm using expected squared jumped distance. *Statistica Sinica*, 20:343–364.

Plummer, M., Best, N., Cowles, K., and Vines, K. (2006). CODA: Convergence diagnosis and output analysis for MCMC. *R News*, 6(1):7–11.

Roberts, G. O., Gelman, A., and Gilks, W. R. (1997). Weak convergence and optimal scaling of random walk Metropolis algorithms. *The Annals of Applied Probability*, 7(1):110–120.

Roberts, G. O. and Rosenthal, J. S. (1999). Convergence of slice sampler Markov chains. *Journal of the Royal Statistical Society B*, 61:643–660.

Roberts, G. O. and Rosenthal, J. S. (2002). The polar slice sampler. *Stochastic Models*, 18(2):257–280.

Roberts, G. O. and Rosenthal, J. S. (2007). Coupling and ergodicity of adaptive Markov chain Monte Carlo algorithms. *Journal of Applied Probability*, 44:458–475.

Roberts, G. O. and Rosenthal, J. S. (2009). Examples of adaptive MCMC. *Journal of Computational and Graphical Statistics*, 18(2):349–367.

Spiegelhalter, D., Thomas, A., Best, N., and Gilks, W. (1995). *Bayesian inference Using Gibbs Sampling Manual Volume i*. MRC Biostatistics Unit.

Straatsma, T. P., Berendsen, H. J. C., and Stam, A. J. (1986). Estimation of statistical errors in molecular simulation calculations. *Molecular Physics*, 57(1):89–95.

Thompson, M. B. and Neal, R. M. (2010). Covariance-adaptive slice sampling. Technical Report 1002, Dept. of Statistics, University of Toronto. arXiv:1003.3201v1 [stat.CO].

Tibbits, M., Groendyke, C., and Haran, M. (2010). Automated factor slice sampling. Talk at 2010 Joint Statistical Meetings in Vancouver.

Wei, W. W. S. (2006). *Time Series Analysis: Univariate and Multivariate Methods, Second Edition*. Pearson/Addison Wesley.